



RYERSON UNIVERSITY

FACULTY OF ENGINEERING, ARCHITECTURE AND SCIENCE

DEPARTMENT OF MECHANICAL AND INDUSTRIAL ENGINEERING

MEC 825 – Mechanical Design

Final Project Report

Friday, April 9<sup>th</sup>, 2021

## Microfluidic Particle Separation

Cloud Capstone

Faculty Advisor: Dr. Scott Tsai

Team Members: Yara Abdul-Ghani 500740781

Jasper Ian Sagulo 500837793

James Yamson 500832942

Syed Shoaib Hasan 500832412

## Abstract

Particle separation application methods have been increasingly used in many industries such as the healthcare and food industry for clinical research or detecting bacteria. The most commonly used separation methods are active techniques which use electric and magnetic fields which alters the particles properties. This report will explore different passive techniques such as Cross-Flow Filtration, Dean Flow Fractionation and Pinched Flow Fractionation designed to separate two particles with  $1.5\mu\text{m}$  and  $3.75\mu\text{m}$  radii and  $1 \cdot 10^{-12}\text{ kg}$ . Following the system analysis of the lab-of-a-chip, alternative design concepts were generated and simulated using COMSOL Multiphysics simulation software. The aim of this project is to design a solution with enhanced particle separation distance. After the evaluation of alternative designs based on particle separation distance, particles per second throughput and manufacturability, concept 2 was chosen as the final design solution. Concept 2 consists of a serpentine flow channel with added buffer flows, which enhances particle separation distance. The separation distance was found to be  $7.59\mu\text{m}$  and the convergence test had a percentage difference of 1.45%

## Table of Contents

<b>Abstract</b>	<b>1</b>
<b>Table of Contents</b>	<b>2</b>
<b>List of Figures</b>	<b>7</b>
<b>List of Tables</b>	<b>8</b>
<b>1.0 Introduction</b>	<b>9</b>
<b>2.0 Literature Review &amp; Background Research</b>	<b>10</b>
2.1 Lab-on-a-Chip	10
2.2 Microfluidics Fundamentals	10
2.3 Flow Cytometry	13
2.4 Particle Separation	15
2.4.1 Pinched Flow Fractionation	16
2.4.2 Inertia and Dean Flow Fractionation	17
2.4.3 Micro-vortex Manipulation	18
2.4.4 Deterministic Lateral Displacement	18
2.4.6 Filtration	19
2.4.7 Hydrodynamic Filtration	20
2.4.8 Micro-Hydrocyclone	21
2.5 COMSOL Simulation	22
2.5.1 Procedure	22
2.5.2 Methodology to Simulate and Model	23
2.6 Manufacturability	24
<b>3.0 General Approach to the Problem</b>	<b>25</b>
3.1 Problem Statement	25
3.2 Reference Designs	26
<b>4.0 Design Requirements</b>	<b>31</b>
<b>5.0 System Design</b>	<b>32</b>
5.1 System Diagram	32
5.2 System Interface	33
5.3 System Assumptions	33
<b>6.0 Concept Design</b>	<b>34</b>
6.1 Concept 1 - Cross-Flow Filters with Inertial Focusing	34

6.1.1 Initial Design	34
6.1.2 Final Design	37
6.2 Concept 2 - Serpentine Channel using Buffer Flow	38
6.2.1 Initial Design	38
6.2.2 Final Design	41
6.3 Concept 3 - Pinched Fractionation with Double Buffer Flow	45
6.3.1 Initial Design	45
6.3.2 Final Design	47
6.4 Concept 4 - Spiral Microchannel	48
6.4.1 Initial Design	48
6.4.2 Final Design	51
6.5 Concept Evaluation	52
6.5.1 Results	54
6.5.2 Concept 1	58
6.5.3 Concept 2	60
6.5.4 Concept 3	62
<b>7.0 Conclusion and Recommendations</b>	<b>65</b>
<b>8.0 References</b>	<b>66</b>
<b>9.0 Appendix A: Detailed Design Drawings</b>	<b>70</b>
<b>10.0 Appendix B: Sample Calculations of Simulation</b>	<b>73</b>
<b>11.0 Appendix C: Data Tables</b>	<b>75</b>
<b>12.0 Appendix D: Particle Throughput Calculations</b>	<b>79</b>
<b>13.0 Appendix E: Convergence Test Calculations</b>	<b>80</b>

## List of Figures

Figure 1. Lab-on-a-chip Device. Sourced from [6]	11
Figure 2. Scaling of Volume vs Surface Area	12
Figure 3. Amount of journal papers and patents up until 2015. Sourced from [1]	12
Figure 4. (a) Pinched Flow Fractionation (b) Asymmetric Flow Fractionation. Sourced from [2]	
18	
Figure 5. Micro-vortex Manipulation Process. Sourced from [2]	19
Figure 6. Deterministic Lateral Displacement Process. Sourced from [18]	20
Figure 7. (a) membrane filtration (b) pillar filtration (c) Weir filtration (d) cross-flow filtration. Sourced from [19]	21
Figure 8. (a) when flow rate of side channel is low (b) when flow rate of side channel is medium (c) when flow rate of side channel is high. Sourced from [19]	22
Figure 9. Micro-Hydrocyclone Device. Sourced from [2]	23
Figure 10. (a) typical cross-flow filter with no buffer flow for hydrodynamic focusing. (b) cross-flow filtration with buffer flow as proposed by Y. Chiu, C. Huang and Y. Lu [21]. Sourced from [21].	27
Figure 11. Microfluidic Filter clogging. Sourced from [19].	28
Figure 12. Three-stage spiral channel with cross-flow filters as parallel channels design proposed by N. Xiang, Q. Li and Z. Ni. Sourced from [24].	28
Figure 13. Symmetric Serpentine Channel [25]	29
Figure 14. Pinched Flow Channel with Sedimentation Forces [24]	30
Figure 15: 5 loop spiral microchannel with 8 outlets [28]	31
Figure 16. System diagram of Lab-on-a-Chip	33
Figure 17. Initial Design of Concept 1	35
Figure 18. Double spiral experiment showing the trajectories of different particle sizes in a spiral channel. Sourced from [33].	36
Figure 19. Velocity Plot with Particle Tracing with Mass for Initial Concept 1. The larger particles are black and the smaller particles are cyan.	37
Figure 20. Final Design of Concept 1	38
Figure 21. Initial Design of Concept 2	39
Figure 22. (Top) Simulation of the serpentine concept with no buffer flow. (Bottom) Simulation of the same concept but with buffer flow. Note: 3.75 $\mu$ m radius particle - Red, 1.5 $\mu$ m radius-Green	40
Figure 23. Particle Tracing with Mass Plot. Top image shows no buffer flow in the serpentine channel loop. Bottom image shows buffer flow in the serpentine channel loop. Note: 3.75 $\mu$ m radius particle - Red, 1.5 $\mu$ m radius- Green	41
Figure 24. Final Design of Concept 2	43

Figure 25. (Top) COMSOL Particle tracing with mass and Streamline results in a serpentine channel without expanding/contracting segments. (Bottom) Particle tracing with mass and Streamline results with expanding/contracting segments.	44
Figure 26. (Top) Velocity gradient of outlet with no sink segment. (bottom) Velocity gradient of outlet with sink segment. (Bottom) Velocity	45
Figure 27. (Top) Velocity gradient of outlet with no sink segment. (bottom) Velocity gradient of outlet with sink segment. (Bottom) Velocity	45
Figure 28. COMSOL particle tracing with mass and streamline results	46
Figure 29. Initial Design of Concept 3	46
Figure 30. Velocity Plot with Particle Tracing with Mass for Initial Concept 3 - Note: 3.75 $\mu\text{m}$ radius particle - Black, 1.5 $\mu\text{m}$ radius- White	47
Figure 31. Final Design of Concept 3	48
Figure 32: 3D plot of spiral microchannel, Note: 20 $\mu\text{m}$ particle - Light green, 6 $\mu\text{m}$ - Red, 10 $\mu\text{m}$ - Dark green	50
Figure 33. Inertial lift and drag forces balancing different sized particles [28]	51
Figure 34. Particle Tracing for Concept 3. Note: 3.75 $\mu\text{m}$ radius particle - Red, 1.5 $\mu\text{m}$ radius particle - Cyan	59
Figure 35. Velocity Plot for Concept 1. Note: 3.75 $\mu\text{m}$ radius particle - Red, 1.5 $\mu\text{m}$ radius- Cyan	60
Figure 36. COMSOL particle tracing with mass and streamline results	61
Figure 37. Velocity Plot for Concept 2. Note: 3.75 $\mu\text{m}$ radius particle - Red, 1.5 $\mu\text{m}$ radius- Green	62
Figure 38. Particle Tracing for Concept 3. Note: 3.75 $\mu\text{m}$ radius particle - Red, 1.5 $\mu\text{m}$ radius particle - Cyan	64
Figure 39. Velocity Plot for Concept 3. Note: 3.75 $\mu\text{m}$ radius particle - Red, 1.5 $\mu\text{m}$ radius- Cyan	64
Figure 40. Detailed Drawing of Concept 1	71
Figure 41. Detailed Drawing of Concept 2	72
Figure 42. Detailed Drawing of Concept 3	73

## List of Tables

Table 2. Concept 1, Average particle separation distance for different starting inlet position of the 3.0 $\mu\text{m}$ diameter particle	55
Table 3. Concept 2, Average particle separation distance for different starting inlet position of the 3.0 $\mu\text{m}$ diameter particle	56
Table 4. Concept 3, Average particle separation distance for different starting inlet position of the 3.0 $\mu\text{m}$ diameter particle	57
Table 5. Summarized Separation Distance	57
Table 6. Summarized Results for Time until 1000 particles pass the separation plane.	58
Table 7. Percentage Difference of Velocity Results of Convergence Test of Concept 1	61
Table 8. Percentage Difference of Velocity Results of Convergence Test of Concept 2	63
Table 9. Percentage Difference of Velocity Results of Convergence Test of Concept 3	65
Table C1. Concept 1, 3.0 $\mu\text{m}$ -diameter Particle Coordinates at Inlet and Penetration of Separation Coordinate Plane	76
Table C2. Concept 1, 7.5 $\mu\text{m}$ -diameter Particle Coordinates at Inlet and Penetration of Separation Coordinate Plane	77
Table C3. Concept 2, 3.0 $\mu\text{m}$ -diameter Particle Coordinates at Inlet and Penetration of Separation Coordinate Plane	77
Table C4. Concept 2, 7.5 $\mu\text{m}$ -diameter Particle Coordinates at Inlet and Penetration of Separation Coordinate Plane	78
Table C5. Concept 3, 3.0 $\mu\text{m}$ -diameter Particle Coordinates at Inlet and Penetration of Separation Coordinate Plane	79
Table C6. Concept 3, 7.5 $\mu\text{m}$ -diameter Particle Coordinates at Inlet and Penetration of Separation Coordinate Plane	79

## 1.0 Introduction

One of the most important advancements in the biomedical industry in recent times has been the creation of microfluidic lab-on-a-chip systems. These single chipsets can be used for various analyses including single cell studies, DNA sequencing, and drug testing. While lab-on-a-chip systems in general cover analyzing and processing fluids at the micro-scale, it's the geometry that exploits the physical phenomena to achieve the mixing, sampling, dispensing, and separating particles at that scale that brings interest to other fields from physics and engineering backgrounds. A particular area of interest is within microscale flow cytometry; separating two or more particles based on size and biological properties, particularly useful for cell sorting, enrichment, and isolation. While accomplished in the past by electromagnetic means such as “tagging” the particle to be magnetized, or give off an electric dipole within an electric field, the downside to these so called “active” techniques are the changed properties of the particle that make it difficult to analyze further, in applications such as point of care diagnostic tools and drug testing. The contrary “passive” techniques, in which no properties of the microparticles are changed but where the microfluidic channel geometry is designed to exploit physical phenomena to achieve particle separation, such as inertial focusing, will be employed to create a new design. More specifically, after researching some preliminary designs of current passive techniques, a new microfluidic channel geometry will be made to separate Erythrocytes and Thrombocyte particles, with the added constraint of a 1000 particles/second throughput benchmark. The process of choosing the right geometry will be done by comparing concepts at the same flow conditions, measuring particle separation, and convergence testing.

## 2.0 Literature Review & Background Research

### 2.1 Lab-on-a-Chip

Lab-on-a-chip is a small device made up of channel systems that are connected to tubing systems containing fluids. The main functions of the device include mixing, sampling, dispensing and separation of particles [6]. Lab-on-a-chip is utilized as a quick method to refine and test development of drugs. This technology uses small volume of liquids, which reduces the amount of time that is required to examine a product. Size of channels are estimated to be a few micrometers that handle volumes that are less than a microlitre. Examining liquids at such a microscale allows researchers to control molecular interactions and concentration and reduce the amount of reagents that are needed to perform an experiment [7]. Lab-on-a-chip can be utilized in various applications such as point-of-care diagnostic tools and drug testing. This technology is fabricated using photolithography and substrates such as glass, silicon and polymers with low fabrication costs [8].

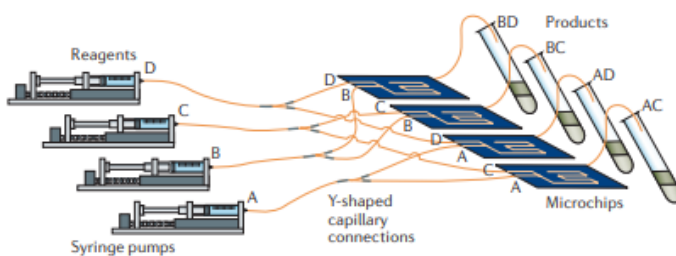


Figure 1. Lab-on-a-chip Device. Sourced from [6]

### 2.2 Microfluidics Fundamentals

Microfluidics revolves around the study of fluid systems at the micron level of length scale. Due to scaling laws, the behaviour of fluid at such a scale differs from that at the macroscale. Scaling down to microscale causes some dominant factors at macroscale to be less dominant while non-dominant factors become dominant. An example would be how scaling works for volume and surface area. Volume scales as  $L^3$  while surface area scales as  $L^2$ . Referring to Figure 2, volume at a larger scale will always be more significant than surface area but at the

smaller length scale, surface area dominates [1]. Additionally, Reynolds number is commonly less than 10 and as a result, viscous forces become more significant [9].

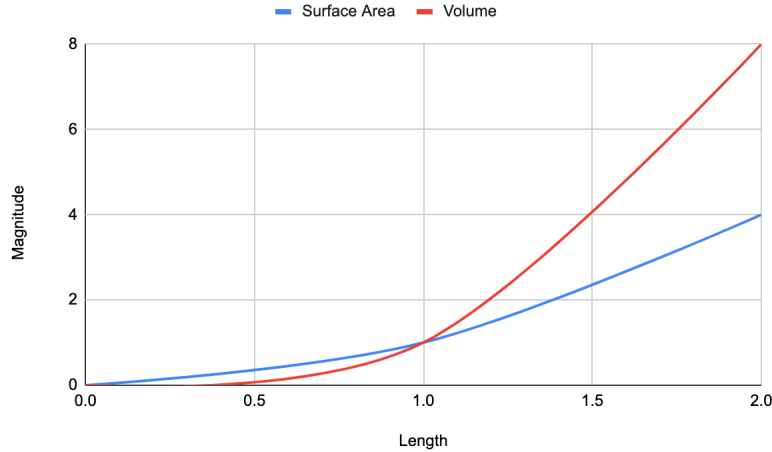


Figure 2. Scaling of Volume vs Surface Area

The phenomenon that occurs at the microscale provides such a wide range of applications that the amount of papers and patents has only been on the rise for the past few decades as shown in Figure 2. These applications are especially useful in the area of biotechnology ranging from single cell analysis through droplet microfluidics, point of care diagnostic through paper and toner based microfluidic systems, and the fabrication of nanoparticle drug delivery [10], [11], [12].

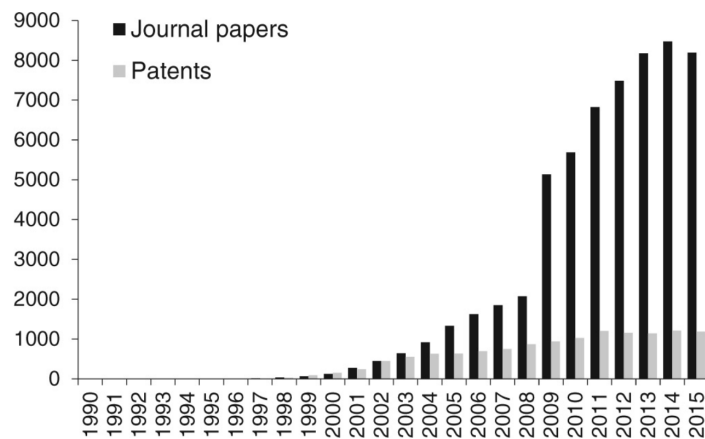


Figure 3. Amount of journal papers and patents up until 2015. Sourced from [1]

For fluids that are steady, incompressible, and have negligible friction due to viscous forces Bernoulli's equation (1) can be used [31]. To clarify, steady refers to the flow parameters, such as density, not changing over time [31]. Incompressible refers to density being constant along the fluid flow regardless of pressure changes [31].

$$\frac{v^2}{2} + gz + \frac{p}{\rho} = \text{const.} \quad (1)$$

To be able to analyze the fluid behaviour at microscale using the conservation laws of mass, momentum and energy, the approach must assume that the fluid behaves as a continuum [13]. The assumption assumes that fluid properties vary continuously in space. For example, using density of a fluid as property of interest at macroscale, increasing the sample volume would more likely include more molecules within the volume. As a result, density would vary smoothly as the sample volume increases [9]. At a smaller length scale, the density scaling becomes chaotic because increasing sample volume would or would not involve molecules within its space. Therefore, the continuum assumption breaks down at a smaller length scale. For most situation, liquid can be seen to have a continuous behaviour at length scale of 10 nm or greater [13]

The equations from the conservation laws of mass, momentum and energy are differential equations in which they require boundary conditions to solve. One of such fluid to solid interface boundaries is the flow velocity in which there is either slip or no slip. In general, it is common to assume no slip boundary for length scales above 300 nm for microfluidic devices with incompressible fluids for it is negligible [1]. Other boundary conditions would depend on the microfluidic device parameters for its inlet and outlet. With a set of boundary conditions and assumptions, one can use the Continuity and Navier Stokes equation to describe the flow of the fluid. Assuming an incompressible and newtonian fluid with no slip, the continuity and navier stokes equation becomes the following:

$$\nabla \cdot u = 0 \quad (2)$$

$$\rho \frac{\partial p}{\partial t} + \rho u \cdot \nabla(u) = -\nabla p + \nabla \cdot (\mu(\nabla u + \nabla u^T)) + F \quad (3)$$

(2) acts as Newton's second law of fluid motion in which the left hand side is the inertial force and the right hand side terms are pressure, viscous and external forces respectively [14]. Solving these equations will provide the pressure and fluid velocity gradient.

## 2.3 Flow Cytometry

Flow cytometry is an all encompassing technology that offers the ability to physically separate subpopulation of cells and analyze them. They scan single particles/cells flowing in a liquid medium past an excitation light source, specifically either a 633 nm He–Ne laser or a 488 nm argon ion laser, due to their limited divergence [15]. As the cell passes through the laser, it scatters light at different angles and emits fluorescence, both of which are used to detect and isolate specific cells consisting of specific properties. Note that there is not a physical separation happening here as opposed to the microfluidic channel; a sample of mixed cells are simply analyzed for their contents and discarded. To understand them in more detail, they will be broken down into four systems: fluidics, illumination, optical/electronic, and data storage/computer control [16].

Within the flow cytometer, cells have to pass through an excitation source individually, a process known as hydrodynamic focusing. It works by creating two walls of a sheath fluid that have the same flow rate, preventing them from mixing together, along with a low Reynolds number ensuring coaxial laminar flow and no slip condition of the wall [17]. Other techniques include using a converging cone shape to reduce cross sectional area and push cells in a single orderly fashion, although some care has been taken when picking the right dimensions of the nozzle and cross-sectional area. For example, before the sample cell passes through the nozzle, it has to be pressurized and injected into a sheath core flow . If there is too high a sample pressure more cells will move through the stream, decreasing the quality of the sample analysis. It is said that the nozzle aperture should be 50-2000 microns after being calibrated to provide a stable

fluidic system [15]. Finding the right balance between channel width, nozzle aperture, and sample pressure, amongst other parameters will be a key focus when coming up with concept designs. While there are other focusing methods, such as acoustic focusing, which aligns cells by sound waves, simulating it on software COMSOL will likely prove to be difficult, so the conventional hydrodynamic focusing method will be used.

After being hit with a laser beam, light scatters around the cell in the forward, and side directions, along with emitting fluorescent lights. The properties of this excitation light source are important because the light scattering at this scale is proportional to certain cell properties listed in the next system. So the ability to homogeneously illuminate cells despite their orientation is of importance, and the most widely used one for this purpose is the argon ion laser configured to work in the visible spectrum [16]. The key takeaway here is that, once separated, orientation of the cells will not be a factor when testing in a flow cytometer.

From the scattered light and emitted fluorescence there are up to 5 parameters to be collected: forward scatter (parallel to the laser beam), side scatter (normal to the laser beam), and measuring three different types of fluorescent emissions. Forward angle light scatter (FSC) is proportional to the cell size in this scale, whereas the side angle light scatter (SSC) is indicative of the granularity or complexity of the cell [16]. So after the forward scatter of the cell, it is gathered by a collection lens and directed towards a photodiode, which turns into an electrical pulse. Larger the particle, larger the FSC, larger the electronic pulse, which are amplified to be converted to a digital form, in essence, “tagging” them. Similarly in SSC, the collection lens is located  $90^{\circ}$  to the intersection, and a fraction of it is directed towards a high sensitivity detector as only 10% of the emitted light accounts for side scatter [16]. This detector converts the electronic pulse to a digital reading like in FSC, and now the cell population can be categorized by size and granularity. There is also the ability to detect fluorescence from 3 different regions of the visible spectrum, where the emitted light is directed towards optical filters and amplified similarly to the process in SSC. These three fluorescent channels are set on a range of wavelengths, and are useful in fluorescence activated cell sorting (FACS), where antibodies with

fluorophore are used to separate cells with specific proteins, but it is not relevant to our case as the team is only dealing with passive techniques for particle separation [16].

The last system, data and computer control, have to do with calibrating instruments, adjusting sensitivities, and making sense of the data that comes out. Using data from the previous system, the FSC and SSC values can be plotted in a histogram to distinguish various cellular subpopulations in a heterogeneous sample, or allow discrimination of cellular debris. While the team will not be dealing with these types of data as the team is not focused on active techniques such as MT-DACS that require counting using a flow cytometer, it is nevertheless interesting to see how a flow cytometer uses scaling laws to detect different cells in a sample, and might be useful to the development of our microfluidic channel [2].

## 2.4 Particle Separation

Particle separation is one of the main functions of a Lab-on-a-chip. Size-based particle sortation is performed in various industries such as industrial production, environmental assessment, food industry, chemical and biological research. For example, in the food industry, harmful bacteria are usually found in food processing stages. As a result, particle separation techniques are utilized to reduce bacteria. Additionally, particle separation is crucial in applications such as chemical syntheses, mineral processing, and biological analyses to divide micron-sized objects in consumer products. One of the main benefits of particle separation is having the ability to separate cells based on their physical properties such as size and volume. Various diseases can alter cell characteristics, so this technique is widely utilized in the healthcare and research industry since diseases, such as cancer, make healthy cells grow in size. Pharmaceutical, cosmetic, and food industries use volume-based particle separation of cells to ensure consistent product quality through the development of digital microfluidics [2].

Particle separation and sorting can be classified into three categories; passive techniques, active techniques or the combination of both passive and active techniques. Active sorting techniques include the usage of an external field to separate particles. On the other hand, passive sorting techniques use the activity between particles, microchannel structures, and flow field.

The efficiency, throughput, and applications of several passive techniques will be discussed below [2].

#### 2.4.1 Pinched Flow Fractionation

Pinched Flow Fractionation is a technique used when particles are continuously changing in size due to laminar flow in a microchannel. In PFF technique, it is assumed that a fluid is incompressible and has a low Reynold number and no-slip condition. Particles are also assumed to be stable and not interfere with fluid flow or the walls of the microchannel. The microchannel in this technique consists of a pinched segment which makes particles move to the sidewall due to the flow rates of fluids. Usually in laminar flow, smaller particles are placed closer to the channel wall whereas larger particles are placed towards the center of the channel due to the center of mass of the particles. The number of particles used does not alter the separation efficiency of this technique. However, the quality of this technique depends on the size of the particles due to flow rate distribution at inlet branches. The PFF quality is also dependent on the shape of the pinched segment and transition from pinch to the board. The width of the pinched segment is also dependent on the particle size. Outlet branches are placed symmetrically to the pinched segment which results in equal fluidic resistances in all branch channels and uniform distribution of fluid. If a particle has an equal diameter to the pinch segment, it will move towards the center of the branch channel. Particles with diameters less than the width of the pinched segment will get separated using this method [2].

In cases where the outlet branches are placed asymmetrically to the pinched segment, this case is called asymmetric PFF. In asymmetric PFF, branched channels are arranged over the pinched segment where one branch is different in size which reduces fluidic resistance in that channel. This channel is called the drain channel since most liquids end up flowing into it. In the asymmetric PFF technique, particles in all sizes can flow into all branches unlike the PFF technique [2].

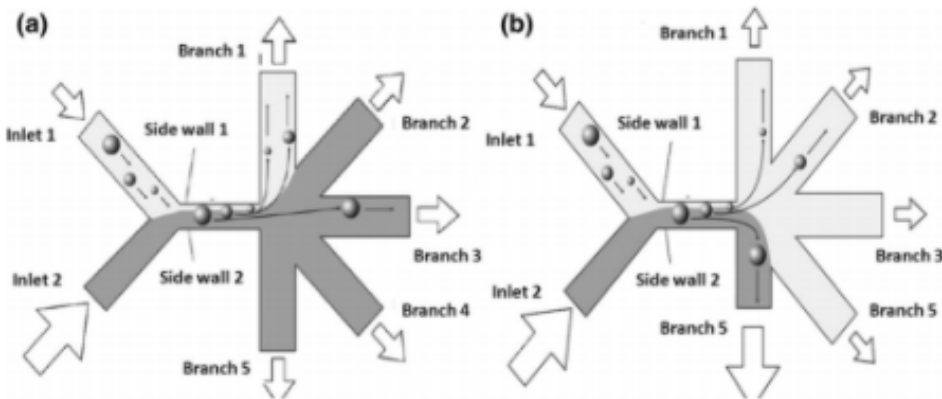


Figure 4. (a) Pinched Flow Fractionation (b) Asymmetric Flow Fractionation. Sourced from [2]

#### 2.4.2 Inertia and Dean Flow Fractionation

This technique utilizes two inertial lift forces that act on the particle: wall effect induced lift force and shear gradient induced life force. The wall effect induced lift force occurs when an asymmetric wake is formed around a spherical particle and when the flow field gets disturbed by the presence of a wall. Shear gradient induced life force happens as a result of the parabolic nature of velocity inside the channel. When the particle is close to the centerline of the channel, the velocity gradient is higher than on the side wall so the particle ends up rolling from the center towards the channel wall [2].

When particles are placed in a straight microchannel, they will move to the wall due to inertial force as a result of the vortex flow created at the expansion region. At the expansion chamber, wall effect induced lift force caused by the sidewalls is weaker than the shear gradient induced lift force. This happens because of the long distance from the mainstream to the sidewalls. Particles moving at the centerline will be pushed towards the sidewalls due to shear gradient induced lift force [2].

The “Dean flow” occurs when a curved microchannel is utilized which generates centrifugal effects. Fluid pressure at the inner walls are higher than at the outerwall, therefore, the fluid at the center is pushed outwards and the fluid at the top and bottom walls move inwards due to the conservation of mass. The swirly secondary flow generated affects the equilibrium

position of the particles which depends on the Reynolds number and ratio of inertial lift force to dean drag force [2].

#### 2.4.3 Micro-vortex Manipulation

Microvortex manipulation technique focuses on separating particles into multiple streams where a number of herringbone grooves are built at the bottom of the channel. Flow of particles is based on the balance between gravitational, buoyancy and hydrodynamic drag forces. A helical flow pattern is formed when a flow is generated over the grooves and vortices are formed. The micro-vortices exert drag forces on particles in both vertical and lateral directions. When the particle is lighter than the medium, the particle will float to the top of the channel due to the balance between upward buoyant, downward drag and gravitational forces. If the particle is heavier than the medium, the opposite will happen; the particles will sink to the bottom of the channel [2].

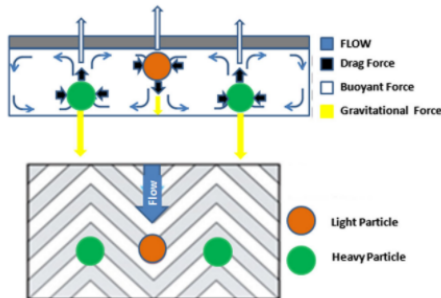


Figure 5. Micro-vortex Manipulation Process. Sourced from [2]

#### 2.4.4 Deterministic Lateral Displacement

Deterministic lateral displacement is a technique that is performed using an array of disposed pillars to navigate the fluid path in a channel. DLD is mainly used in the isolation of blood components, plasma extraction and enrichment of cells. It is also used to evaluate the deformability of particles. When particles are injected into the channel, their trajectory is established by their position in relation to the various streamlines. Particles with critical diameters (cut off diameters) move towards the pillar rows while smaller particles remain in the channel and move in a zigzag trajectory. It was proven that the geometrical parameters of DLD arrays define how the particles are going to flow in the microchannel [18].

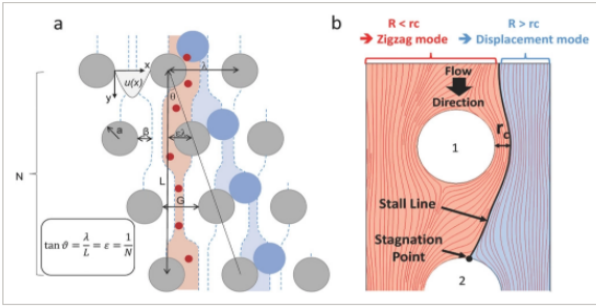


Figure 6. Deterministic Lateral Displacement Process. Sourced from [18]

#### 2.4.5 Zweifach-Fung Effect

The Zweifach-Fung effect states that a particle will follow the high flow rate channel if it reaches a bifurcation region. Bifurcation region is one where a channel splits into two channels with different flow rates. If a particle has a centroid located beyond the critical streamline, it will flow into the channel with the higher flow rate. If a particle's centroid is within the critical streamline, it will flow into the channel with the lower flow rate. Lastly, if a particle's centroid is located at the critical streamline, it will flow into the channel with the higher flow rate due to the Zweifach-Fung effect. The Zweifach-Fung effect generates torque on the particle when shear force acting in the high flow rate direction is more than the shear force in the low rate direction. This causes the particle to move to the branch channel with the high flow rate. The flow rate at which the particle moves into the high flow rate branch is called the critical flow rate which has a ratio of 2.5:1 between the daughter branches for a particle-to-channel diameter ratio of 1.0 [2].

#### 2.4.6 Filtration

Filtration is a method that uses microfabricated filters to separate particles based on their size. There are four types of microfilters that can be used: membrane, Weir, pillar and cross-flow [2]. Membrane filtration is used in many applications such as microfiltration, ultrafiltration, reverse osmosis and gas separation. The process is dependent on hydrostatic pressure difference which generates a driving force which results in some particles passing through the membrane [19]. One of the disadvantages of membrane filtration is the particle accumulation at the filter face which results in a lower separation efficiency. In order to reduce the particle accumulation at the filter, a reverse flow is utilized to clean the membrane. When back-filtration time and feed

concentration are decreased, the average flux increases. Filtration rate is the ratio of hydrostatic pressure difference to its hydrostatic resistance [2]. Membranes are usually made of polycarbonate, nylon, cellulose acetate and anodic aluminium oxide [19].

Weir and pillar filtration methods are used to separate red blood cells, white blood cells, plasma and cancer cells from a blood sample. Pillar filtration utilizes an array of microposts to form size cutoffs. Weir filtration utilizes the capillary effect by having a dam in the flow direction. Cross-flow filtration is similar to Weir filtration and pillar filtration with the only difference is that the fluid flow is perpendicular to the filter structure. This causes hydrodynamic forces on the particle due to filtered flow and the shear flow [19].

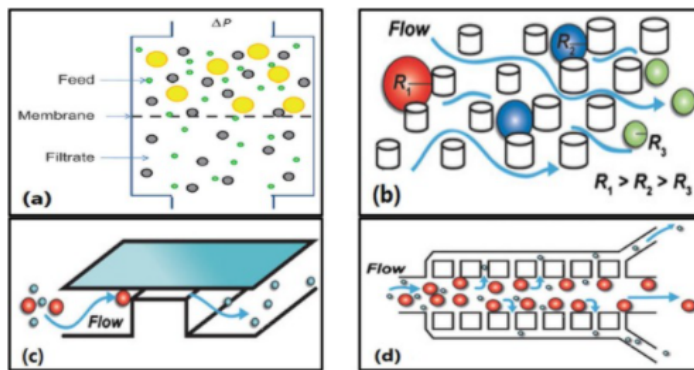


Figure 7. (a) membrane filtration (b) pillar filtration (c) Weir filtration (d) cross-flow filtration.

Sourced from [19]

#### 2.4.7 Hydrodynamic Filtration

Hydrodynamic filtration is similar to cross-flow filtration with the only difference being that in cross-flow filtration, carrier fluid is collected through the side channels whereas in hydrodynamic filtration, particles are collected alongside with the fluid [19]. If the volume flow rate of the side channel is smaller than the flow rate in the main channel, large particles will not be able to flow into the side channel. The inlet branches points are created in order to remove some of the carrier fluid so particles can move to the channel walls. Particles would then move along the side channels depending on their diameter. Particles with a larger diameter are usually collected at the exit channel [2].

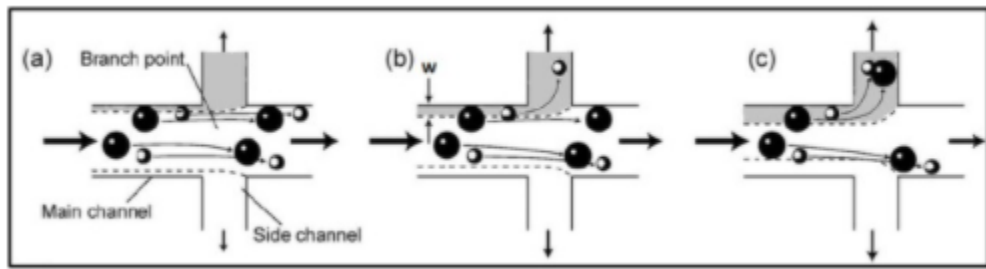


Figure 8. (a) when flow rate of side channel is low (b) when flow rate of side channel is medium (c) when flow rate of side channel is high. Sourced from [19]

#### 2.4.8 Micro-Hydrocyclone

Micro-hydrocyclone is a device that implements particle and liquid separation through utilizing a cylindrical chamber with a frusto-conical bottom and an inlet channel which is tangential to it. Centrifugal force is used to separate particles from liquids. The structure of the micro-hydrocyclone device includes an inlet microchannel, a cylindrical chamber with frusto-conical bottom as the main branch, a top outlet that leads to a microcapillary and a bottom outlet that leads to a microchannel [19]. A crucial element in this device is the vortex finder which is the top outlet capillary extended within the main body of the hydrocyclone. The vortex finder helps the formation of a vortex from the inlet flow. The inlet tangential flow into the cyclone causes a spiral flow pattern which causes the particle-liquid separation due to a net outward radial velocity generated onto the solid particles. A  $\frac{1}{4}$ -28 UNF threaded fittings are used as the interconnection mechanism between the microfluidic chip and the external capillaries. Due to the spiral motion of the fluid, the velocity can be divided into tangential velocity and radial velocity. If a particle circles in the upper cylindrical component of the cyclone, centrifugal, drag and buoyant forces will be exerted onto it [2].

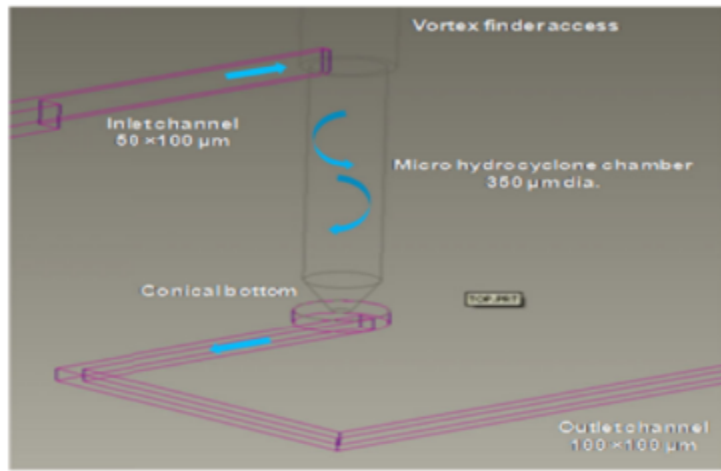


Figure 9. Micro-Hydrocyclone Device. Sourced from [2]

## 2.5 COMSOL Simulation

The COMSOL Multiphysics is a modeling software built upon finite element methods, and can produce solutions to differential equations. After selecting the laminar flow interface, it solves the Navier Stokes equations for complex part geometries that one draws in the software after setting up parameters such as the velocity profile and boundary conditions. While it can be used to model with multiple physics parameters such as magnetic and acoustic interfaces, they are outside the scope of this report. After setting up the parameters, the user builds the mesh and tweaks the size and density to check for convergence. Once there is no discrepancy, the software shows the solution at each node within the microfluidic channel using the boundary conditions provided.

### 2.5.1 Procedure

The procedure for using COMSOL multiphysics to simulate the flow in microscale is fairly intuitive. Initial procedures involve choosing the desired space dimension and physics through “Model Wizard.” In the case of microfluidics particle separation, the model will simulate “Laminar Flow” under “Single-Phased Flow” in three dimensional space. The selection of the physics interface will assign the dependent variables into certain letters and in the case of laminar flow, the dependent variables are the velocity field components and pressure. After selecting the physics for the model, COMSOL will proceed to request for which type of study is

desired. One option being the “Stationary” study applies for when the field properties are not time dependent which will be appropriate for the scope of the report.

Once the preliminary settings are chosen, COMSOL will proceed to display four window interfaces which are the “Model Builder,” “Settings,” “Graphics” and the toolbar. The “Model Builder” provides a tree user interface that lists the items for user based inputs and simulation results. Such user based inputs include “Global Definitions” for any constants or functions, “Geometry” for setting units and solid components, “Laminar Flow” for configuring fluid properties, initial values, boundary conditions, and mesh size, and lastly the results. Selecting an item will project its list of configurations into the “Settings” window allowing for configurations of the model to be made. The “Graphics” window will provide a visual of geometry and the results. It is recommended to check and configure every item in the “Model Builder” to guarantee the most accurate results. Once simulation is over, the result item allows for the selection of which values such as field or pressure gradient to display in the “Graphics” window.

### 2.5.2 Methodology to Simulate and Model

As previously mentioned, to describe the flow of a fluid in the microscale the Navier stokes equation is required. For complex geometries, solving the differential equation will be problematic and time consuming. Therefore, COMSOL is required to be able to observe the flow for it provides finite element analysis. The analysis predicts physical properties through FEM which discretizes the mathematical models to provide a discrete approximation of the system [20]. Since the solution will be an approximation of the DE, there will be an error called “Truncation Error” in which it depends on the model and element size. Moreover, the FEA process involves preprocessing and post processing. Preprocessing refers to the definition of the geometry, domain, material, boundary conditions, constraints and mesh [20]. Post processing refers to the generation of results from the expression and derived values, estimating the error and estimating the sensitivity of the model [20].

## 2.6 Manufacturability

In terms of manufacturability, most single flow with variable height channel geometries, such as those found in our concepts, utilize multi-step photolithography; a technique of engraving a pattern on a substrate using light. A negative outline of a mask is first created, with different layers corresponding to different heights. Using a silicon wafer as a base, negative photoresist is applied on top and is bonded with the silicon wafer. To accommodate the variable height, different manufacturing protocols are used on the developed wafer at different heights, called the flow low, flow high, and Herringbone layer [21]. After applying light when exposed to heat, the wafer resting on top won't dissolve in a solvent called the developer, which is where the negative masks come in to build the pattern. After all that, the mold is inspected to make sure the valves are all aligned to the control lines and inlets.

There have been recent studies that show 3D printing elastomeric structures in the millimeter range is possible by “extruding viscoelastic inks into self-supporting microchannels”, so future possibilities of automating this process is a very real likelihood [22].

## 3.0 General Approach to the Problem

### 3.1 Problem Statement

The most commonly used particle separation technique within microfluidic flow cytometry is done through active techniques which use electromagnetic fields. Electromagnetically tagging a particle changes its properties which can alter results for applications such as point-of-care diagnostic tools and drug testing in the healthcare industry. Moreover, manufacturing a microchannel that utilizes passive techniques is cheaper than an active technique microchannel. Therefore, a new microfluidic channel design will be designed by exploiting the physical phenomena present in current passive separation techniques that exist. This report will outline the steps taken in order to choose a final solution that is efficient and effective. Some deliverables include:

- The design process which outlines design requirements considered when designing a potential solution. Additionally, the system of the lab-on-a-chip will be analyzed in order to generate different concept designs. Concept designs will then be compared and evaluated to choose the optimal solution.
- COMSOL simulation results of alternative design solutions
  - Convergence test for each design
  - Particles path analysis
- Detailed design drawings of alternative design solutions

### 3.2 Reference Designs

Creating microfluidic filters implies utilising reference designs to aid in the design process. Since using reference designs helps in understanding how to create novel designs and geometries to properly apply the passive techniques.

A design that utilizes cross-flow filtration enhanced with hydrodynamic focusing was proposed by Y. Chiu, C. Huang and Y. Lu [21], the design is shown in Figure 10. As can be seen in Figure 10 (a), a typical cross-flow filter has one inlet and two outlets where one outlet is meant for the larger particle and the other is meant for the smaller particle. Also, it will have two particles of different sizes flowing from the inlet. Only particles with diameters smaller than the width of the filters will pass through, however this configuration has a low separation efficiency [21]. This can be attributed to the fact that the particles are spread across the top microchannel and only the smaller particles close to the filters will pass through [21]. As seen in Figure 10 (b), their proposed design adds a buffer flow for the purpose of hydrodynamic focusing [21].

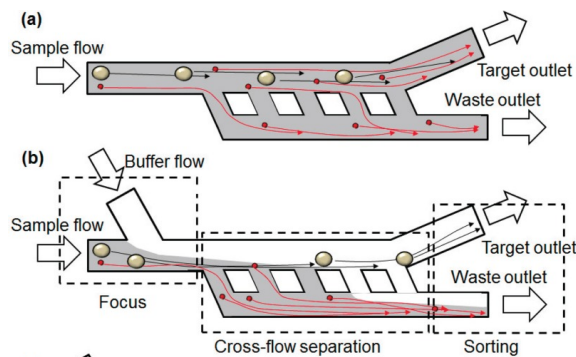


Figure 10. (a) typical cross-flow filter with no buffer flow for hydrodynamic focusing. (b) cross-flow filtration with buffer flow as proposed by Y. Chiu, C. Huang and Y. Lu [21]. Sourced from [21].

To explain, the buffer flow pushes the particles closer to the filters to solve the issue of the smaller particles being spread apart in the top channel and being away from the filter. Their particular design garnered a  $99.2 \pm 0.4\%$  and  $97.9 \pm 0.5\%$  for the small and large particles [19]. Typically, the purity ranges from 90 to 100% [19] so their design was very successful. An issue

that can occur is that if the buffer flow speed is too high relative to the inlet speed the filters will be subject to clogging and membrane fouling as shown in Figure 11.

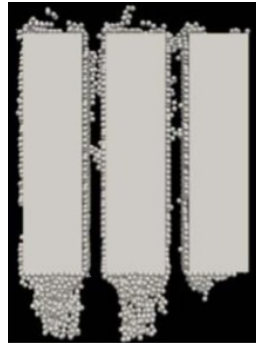


Figure 11. Microfluidic Filter clogging. Sourced from [19].

A design that utilizes inertial microfluidics with cross-flow filtration was proposed by N. Xiang, Q. Li and Z. Ni [25], the design is shown in Figure 12. The forces that push the particles to be the filtration channels is the inertial lift force and wall-induced inertial lift force [25]. The inertial lift force is the net lift force for a shear-gradient-induced inertial lift force [25]. The velocity profile of the fluid flow causes an inertial force on the particles to move towards the filtration channels [25]. Same as for the design in Figure 10, due to the usage of cross-flow filters the design may be subject to clogging and membrane fouling.

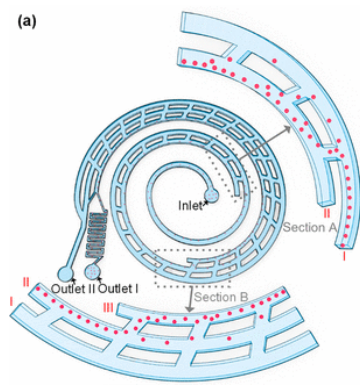


Figure 12. Three-stage spiral channel with cross-flow filters as parallel channels design proposed by N. Xiang, Q. Li and Z. Ni. Sourced from [24].

A design that utilizes inertial lift forces and dean drag force is a serpentine channel and is shown below in Figure 13:

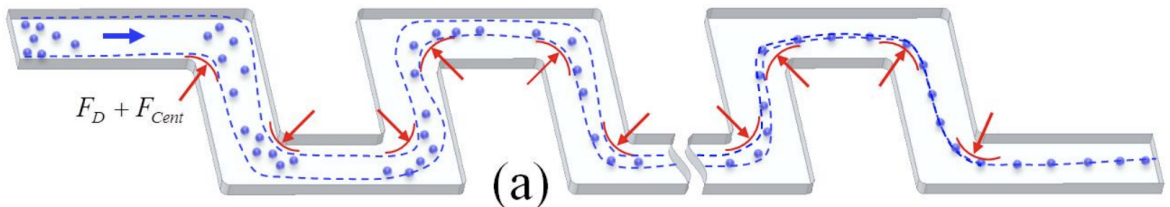


Figure 13. Symmetric Serpentine Channel [25]

A straight channel with a square cross section would have 4 equilibrium positions located on the center of each wall, however alternating symmetric and asymmetric curves reduces it into two and one equilibrium positions respectively [25] . This brings an understanding that the equilibrium position depends on the ratio of dean drag force ( $F_D$ ) and inertial lift force ( $F_L$ ). As a result, the dean drag force serves to reduce the number of equilibrium positions due to the inertial lift forces [25]. Moreover, the alternating direction of the curve facilitates the focusing mechanism. Every curve introduces inertial force, pushing the particle away from the wall but at the same time it also introduces a drag force that pushes it towards the wall [25]. Therefore, increasing the number of alternating curves will reduce the streak width much further. Additionally, purity of the separation is affected by the size of the particles in which below a threshold, the particles remain unfocused [25]. As a result, unfocused small particles may exit the channel the same way as the focused larger particles.

A design that utilizes pinched flow fractionation technique with sedimentation forces is shown in Figure 14.

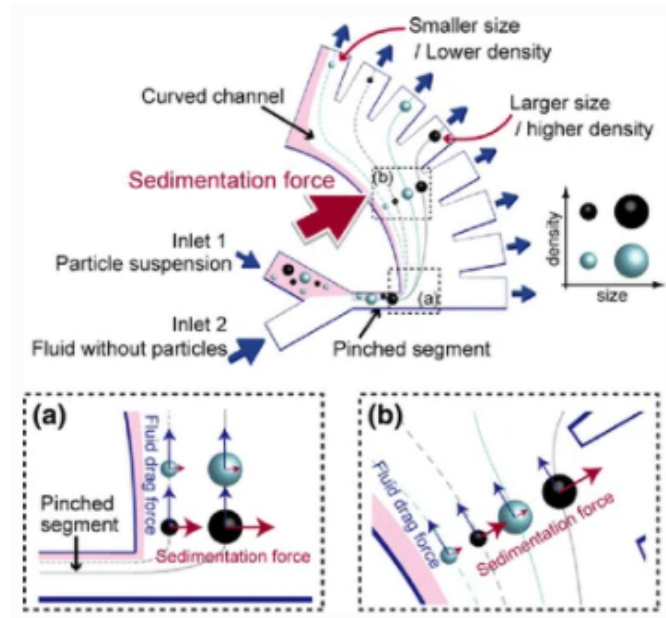


Figure 14. Pinched Flow Channel with Sedimentation Forces [24]

This reference design analyzes a combination of pinched flow fractionation and sedimentation forces for particle separation. It is manufactured utilizing standard soft lithography and molding techniques. This reference design consists of 15 mm wide radius curvature with two inlets and twelve outlets in order to exert strong centrifugal forces and have longer retention time. The inlets of the design are positioned and adjusted to control the inlet flow rates. The volumetric flow rate ratio between inlets 1 and 2 is 1:20. The sedimentation velocity is calculated using the following equation (YA1):

$$U_s = \frac{\rho_p}{18r\mu} D_p^2 U^2 \quad (\text{YA1})$$

where density and diameter of particle, average flow velocity and curvature radius values are examined. This experiment proved that adding sedimentation force can increase the separation distance between particles [24].

A good example of a design that utilizes inertia and Dean flow fractionation for continuous particle separation is shown in Figure 15, proposed by Kuntaegowdanahalli et al [28]:

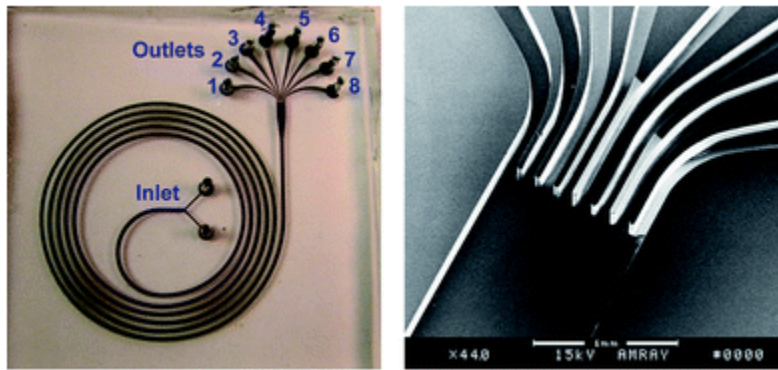


Figure 15: 5 loop spiral microchannel with 8 outlets [28]

Consisting of a “five loop Archimedian spiral microchannel”, it has an initial radius of curvature of 1cm, width of 500 $\mu\text{m}$ , 2 inlets and 8 100 $\mu\text{m}$  wide outlets [28]. It’s height varies from 90-140 $\mu\text{m}$ , as increasing height or De values (flow conditions) changes the particle stream position. The particles tested for separation were 10, 15, and 20 $\mu\text{m}$ , and showed a 1 million cells/min throughput of separation of said neural cells [SH8]. Similar to Concept 1, this design uses both lift and drag forces to focus particles and separate, without the use of any filters. The pros of this design are a wide variety of outlets to make separation of different sized particles easier, flexible dimensions, and the aforementioned high throughput. The only negative is it’s larger area when compared to simpler designs such as PFF, which might mean getting the results will take more time as the particles are travelling larger distances. While the sizes of particles being separated are larger than the 3 and 7.5 $\mu\text{m}$  diameter particles being chosen for the system, manipulating the design so it meets the ratio criteria of  $a_p/D_h \geq 0.07$ , where  $a_p$  is the particle diameter and  $D_h$  is the hydraulic diameter, as well as balancing the lift and drag forces of the particle so they’re in the correct equilibrium position, should allow for those particles to be tested.



## 4.0 Design Requirements

For the design requirements the main categories to consider are functionality, usability, and producibility. Functionality refers to the performance of the design. In terms of functionality requirements the design:

- Must separate particles
  - Channels have a 1000 particles/sec throughput
  - Separate two different sized particles
  - Cell scale (micron scale  $10^{-6}$  metres)
- Must operate without external field (magnetic/electric/acoustic)
  - External Field Strength = 0
  - Usage of passive separation techniques
- Simulation results must converge
  - Result deviation < 10%

Usability refers to users being able use the design safely and intuitively with minimal conditions. So, in terms of usability requirements the design must minimize space it takes on the chip. Producibility refers to the ease of manufacturing and assembly. So, in terms of producibility requirements the design must have a simple cross-section geometry.

## 5.0 System Design

### 5.1 System Diagram

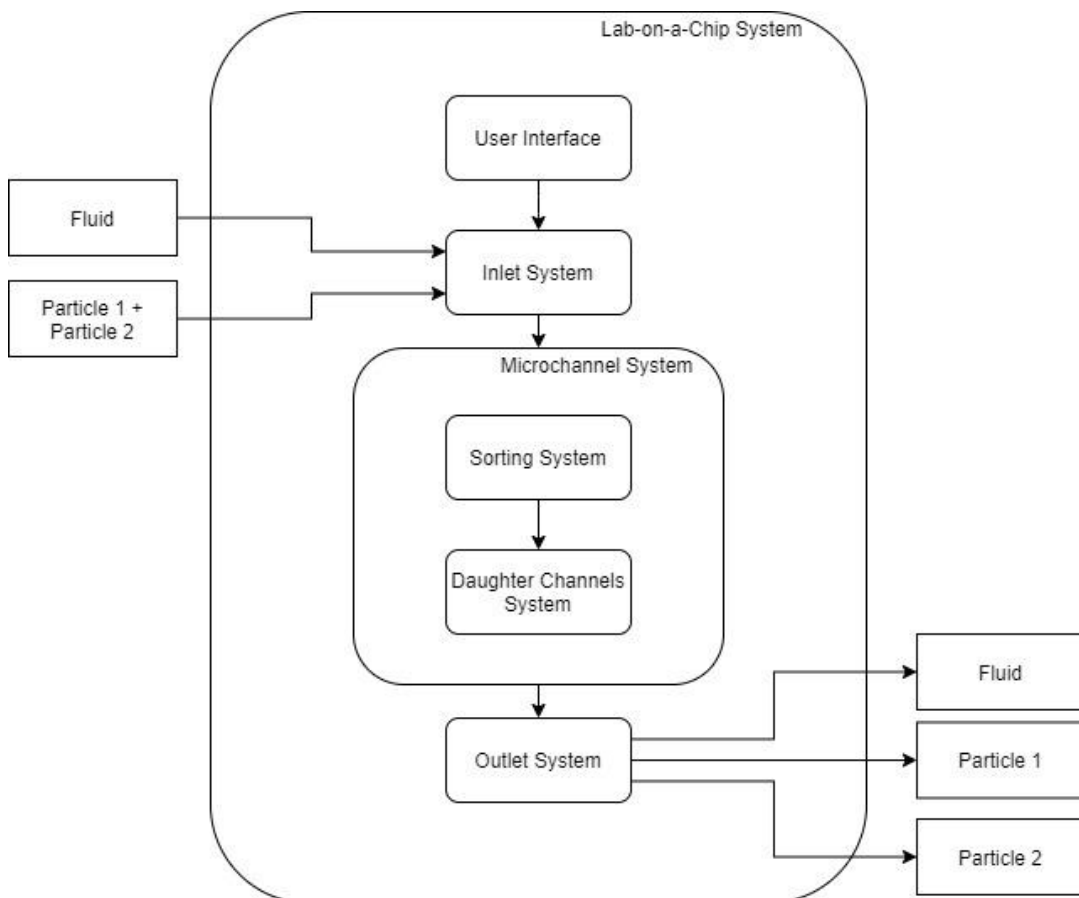


Figure 16. System diagram of Lab-on-a-Chip

Lab-on-a-Chip consists of an inlet system, a microchannel system and an outlet system. The fluid and particles inputs get inserted through the inlet system, which then flows through the microchannel system and get collected at the outlet system. Particles with different mass and density are collected at different outlets.

## 5.2 System Interface

**User interface:** the user chooses what kind of fluid and particles to insert through the inlet system. Particles mass and density can vary and it's important to develop a product that will be able to work with various masses and densities.

**Inlet system:** the user inserts the fluid and particles through the inlet. Multiple inlets or bifurcation channel can be added to the design for enhanced separation distance between both particle streams

**Microchannel system:** the microchannel system is divided into two systems, sorting system, and daughter channels system. The particles flow from the inlet system into the microchannel, where they are separated. The sorting system includes the separation technique used to separate particles based on size and density through different daughter channels.

**Outlet system:** the user collects particles from the outlet system. Multiple outlets will be used as particles with different mass and density will separate and flow to different outlets.

## 5.3 System Assumptions

This system is going to be simulated using COMSOL simulation software where two particles with a mass of  $1 \cdot 10^{-12} \text{ kg}$  and radii of  $1.5 \mu\text{m}$  and  $3.75 \mu\text{m}$  will be analyzed. Assumptions made during the design process are:

- There is a no slip condition at the wall
- Fluid is incompressible and Newtonian
  - Water is used with a density of  $999.8 \text{ kg/m}^3$ , dynamic viscosity of  $1.79 \cdot 10^{-3} \text{ Pa}\cdot\text{s}$ , and temperature of  $273.15\text{K}$
- The flow is laminar with a Reynolds number of 0.1
- Particle-to-particle collision is ignored
- COMSOL simulates the particles as points

## 6.0 Concept Design

### 6.1 Concept 1 - Cross-Flow Filters with Inertial Focusing

#### 6.1.1 Initial Design

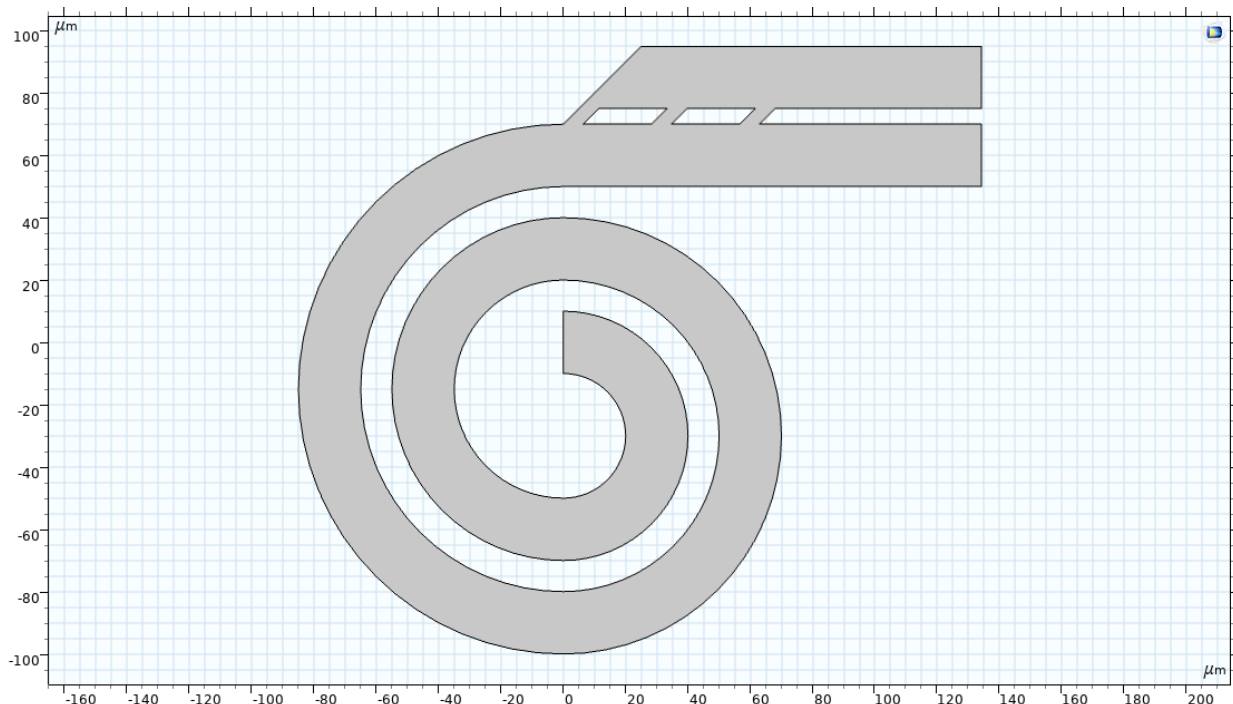


Figure 17. Initial Design of Concept 1

The initial design of concept 1 references features from the proposal design from Y. Chiu, C. Huang and Y. Lu [31] (as seen in Figure 10) and N. Xiang, Q. Li and Z. Ni [32] (as seen in Figure 12). The main passive techniques used are inertial focusing and cross-flow filtration. The inlet is situated at the center and the outlets are the parallel channels at the top right of Figure 17. The spiral channel geometry is used for inertial focusing and the cross-flow filters are near the outlet. The channel width in the spiral channel and parallel channels near the outlet are  $20\mu\text{m}$  wide. The cross-flow filters are  $6.364\mu\text{m}$  wide and  $28.28\mu\text{m}$  apart. The initial design was made in 2D.

Inertial migration (similar to what was used in the N. Xiang, Q. Li and Z. Ni reference design) is used instead of using a buffer flow (similar to what was used in the Y. Chiu, C. Huang and Y. Lu reference design) for hydrodynamic focusing. To explain, particles move laterally to specific equilibrium paths in the spiral channel depending on their size, the channel geometry, and the flow conditions [33]. Furthermore, the smaller particles in the spiral channel will be closer to the walls of the spiral channel relative to the larger particles due to the inertial lift forces as shown in Figure 18.

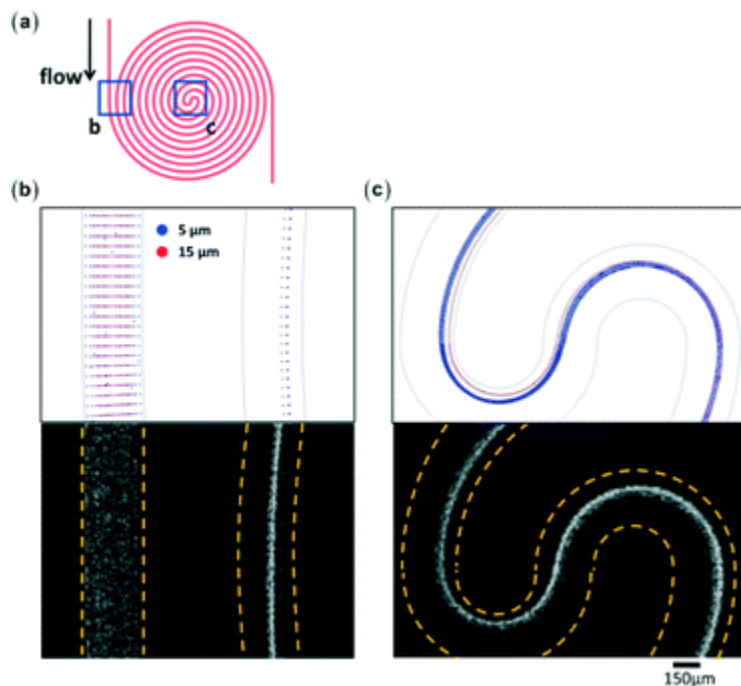


Figure 18. Double spiral experiment showing the trajectories of different particle sizes in a spiral channel. Sourced from [33].

Since the smaller particles move closer to the wall this rectifies one of the issues the typical cross-filter has which is that smaller particles in the main microchannel that are far from the filter do not move through the filter [21]. With the smaller particles closer to the wall they will move through the cross-flow filters due to the pressure difference between the main microchannel and filters [34].

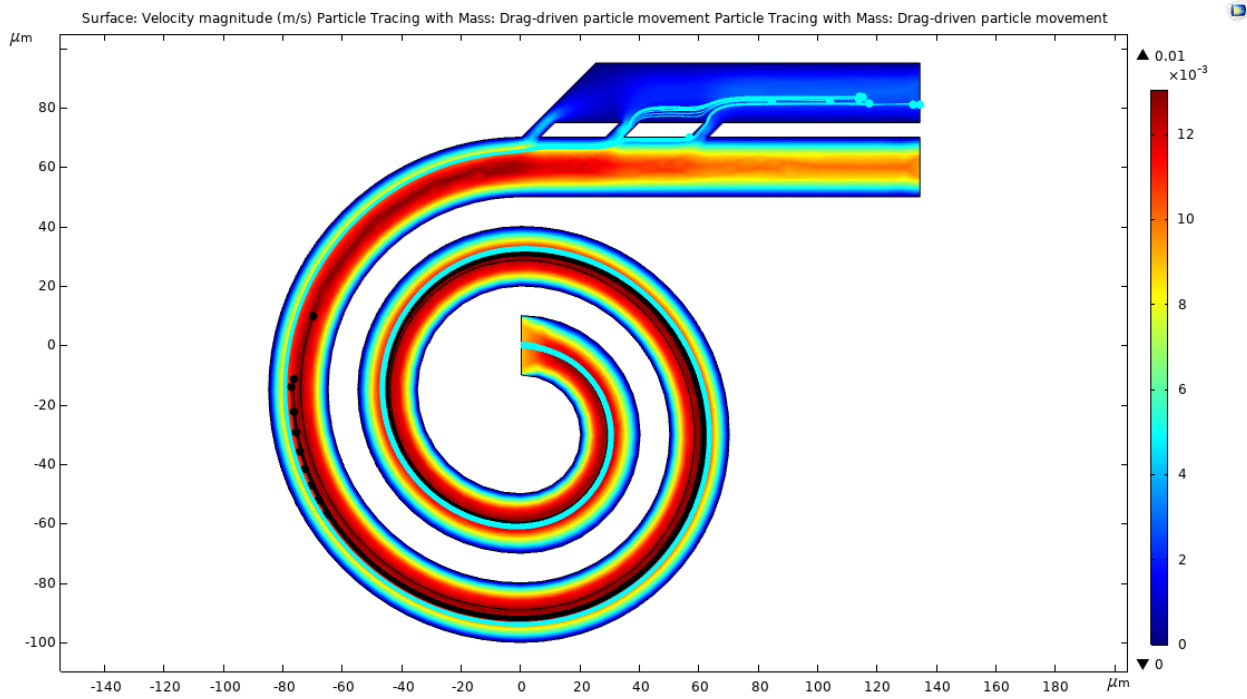


Figure 19. Velocity Plot with Particle Tracing with Mass for Initial Concept 1. The larger particles are black and the smaller particles are cyan.

As seen in Figure 19 is a sample simulation in 2D using the system assumptions. The particles did not reach the outlet which can be attributed to the geometry or the flow speed. However, the smaller particles moved closer to the wall relative to the larger particles as a result of the inertial focusing of the spiral geometry. Also, the smaller particles move through the filters due to them being closer to the wall. Thus, the theory pertaining to the design of the initial concept is verified.

### 6.1.2 Final Design

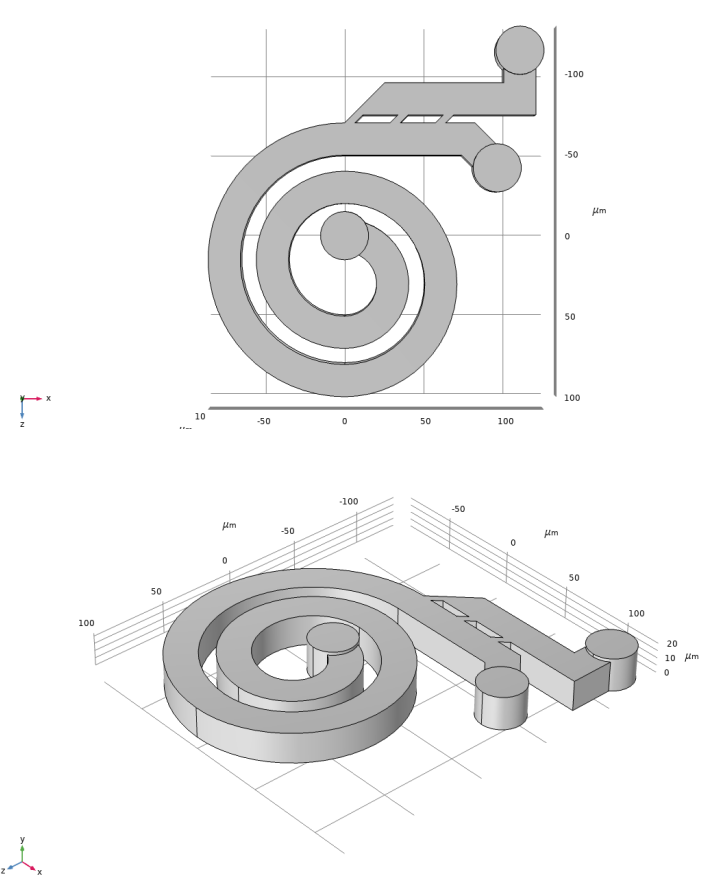


Figure 20. Final Design of Concept 1

For the final design of concept 1, Figure 20 shows the 3D design of the concept. In the initial design, the particles did not reach the outlet so to rectify the issue the geometry was changed. That is to say, the length of the cross-flow section was shortened and the inlet and outlet geometry was changed to have a circular cross section of  $30\mu\text{m}$  diameter. By decreasing the path length to the outlet it allows the particles to reach the outlet. Since the smaller particles in the initial design did not reach the outlet at all. Also by changing the geometry of the inlet and outlet the particles will be able to move along the channel faster.

$$Q = VA_c \quad (2)$$

This is due to increasing the inlet from a  $400\mu\text{m}^2$  rectangular cross-section to a  $707\mu\text{m}^2$  circular cross-section. Assuming the flow rate stays constant, the velocity will increase as the cross-sectional area decreases as per (2). Thus, the particles will move faster along the inlet.

## 6.2 Concept 2 - Serpentine Channel using Buffer Flow

### 6.2.1 Initial Design

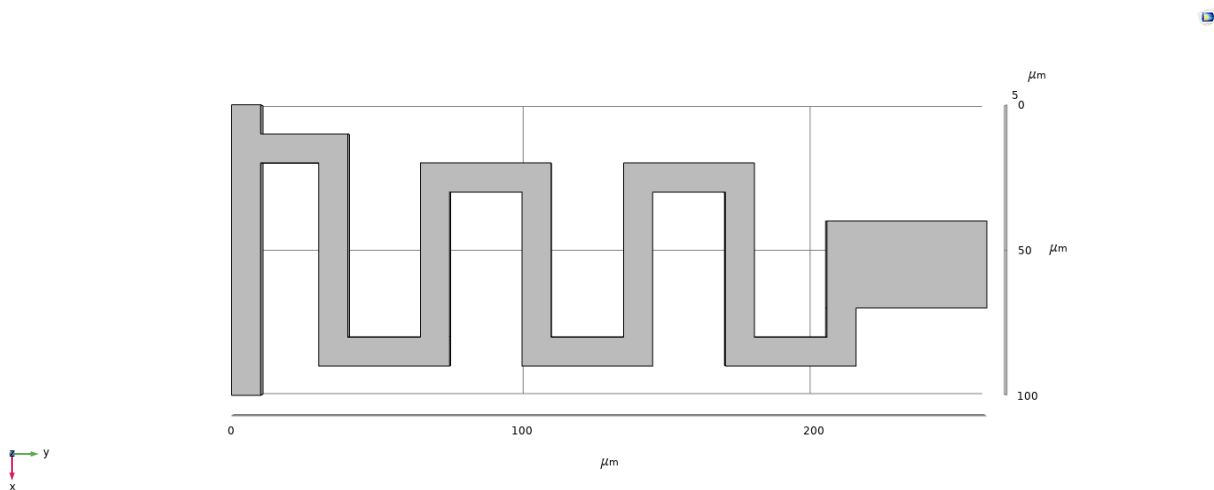


Figure 21. Initial Design of Concept 2

Initial concept 2 involves a slight modification of the symmetric serpentine channel concept from reference design in which the sample and buffer inlets are located on the top left and bottom left respectively. The modification adds a buffer flow to focus the particles towards the negative-x side. This addition facilitates the focusing of the larger and smaller particles with their respective equilibrium positions. Such an effect is evident based on the simulation in Figure 22.

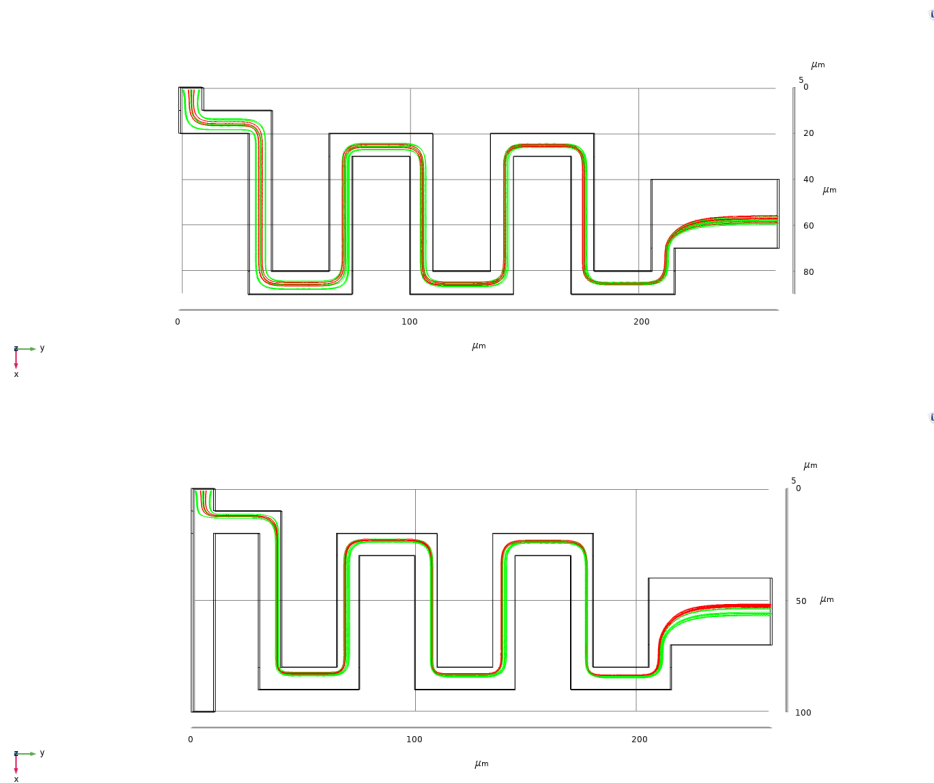


Figure 22. (Top) Simulation of the serpentine concept with no buffer flow. (Bottom) Simulation of the same concept but with buffer flow. Note: 3.75 $\mu\text{m}$  radius particle - Red, 1.5 $\mu\text{m}$  radius-Green

Based on Figure 22, the equilibrium positions of the two types of particles in the simulation with no buffer flow shows overlap all throughout the channel. In contrast, the simulation with buffer flow shows the separation of the equilibrium positions by the end of the pattern.

Figure 23 provides a closer view of the particle trajectories to see the mechanism much clearer. To provide context for Figure JS4, the equilibrium positions caused by balance in centrifugal and viscous drag force will alternate between overlapping and separating which is due to the alternating nature of the geometry and an asymmetric starting point. It may sound counterintuitive however, with every cycle of the “zig-zag” pattern the particles are increasingly more focused with their respective equilibrium position due to the increasing exposure to the

inertial and drag forces [23]. As a result, the separation of the equilibrium positions becomes clearer. Looking back at Figure 23, the point of overlapping and separation differs between with and without buffer flow which is due to a combination of different starting systems. The channel with no buffer flow will have separation of the equilibrium positions at every vertical channel with respect to the channel orientation in Figure 22. In terms of the channel with buffer flow, the equilibrium position begins and maxes out at every other horizontal and vertical channel. Comparing the two will clearly show that the channel with buffer flow provides a much clearer separation of the equilibrium positions at the same amount of loop.

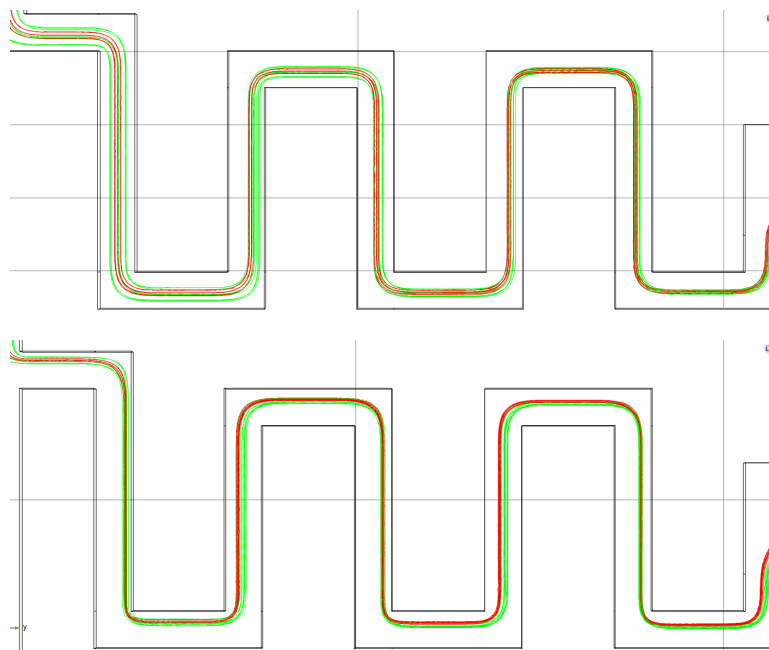


Figure 23. Particle Tracing with Mass Plot. Top image shows no buffer flow in the serpentine channel loop. Bottom image shows buffer flow in the serpentine channel loop. Note:  $3.75\mu\text{m}$  radius particle - Red,  $1.5\mu\text{m}$  radius- Green

The reason for the improvement is due to the fact that the particles are initially pushed towards an extreme side of the channel. As those initially focused particles navigate around the first bottom left curve in Figure 23, the particles are pushed towards the center of the channel due to the centrifugal force at which the inner corner experiences [25]. Due to the difference in size and density, the centrifugal force will be higher in the more dense particle ( $1.5\mu\text{m}$  radius) [25]. As a result, the  $1.5\mu\text{m}$  radius particle will traverse more towards the outer corner in comparison

to the  $3.75\mu\text{m}$  radius particle. Additionally, the centrifugal force the particle experiences is directly and indirectly proportional to the particle tangential velocity and average radius of orbit respectively. Also the particle tangential velocity decreases as it moves from the inner to the outer corner [23]. However, because the particles are still closer to the inner corner after the first turn, the following turn introduces another centrifugal force which further increases the equilibrium positions.

In terms of the serpentine channel with no focusing flow, the particles enter the first loop mostly distributed much wider across the channel. The particles will also experience centrifugal movement however, the majority of the particles will experience a lower magnitude of centrifugal force due to the increasing radius of orbit and decreasing tangential velocity towards the outer corner [23 ]. As a result, there will be a lower difference in centrifugal force between the two particles to separate the equilibrium positions.

### 6.2.2 Final Design

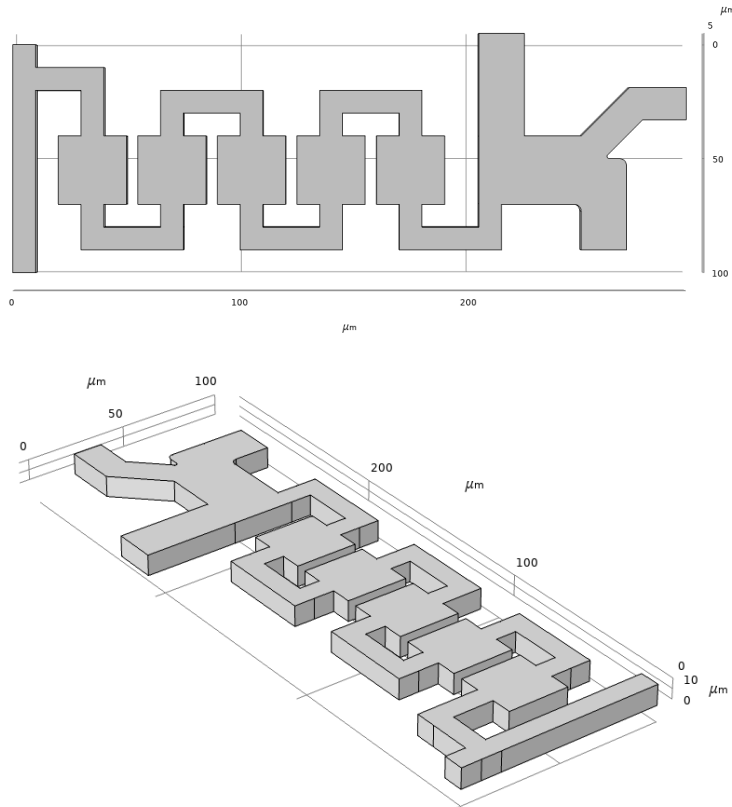


Figure 24. Final Design of Concept 2

The final design came to be after the addition of expanding and contracting sections to refine the serpentine channel and a bifurcation system to provide dedicated outlet channels for the two different particles.

Firstly, the expanding and contracting segments were added to reduce adding more loops into the channel. The segments, similar to the zig zag pattern induce centrifugal movement onto the particles but only at little arc length. Smaller arc length will focus the particles much less however by adding them within each loop, it will equate to adding more another loop or more without actually doing so. The improvement of the focusing is evident as shown in the comparison in Figure 24.

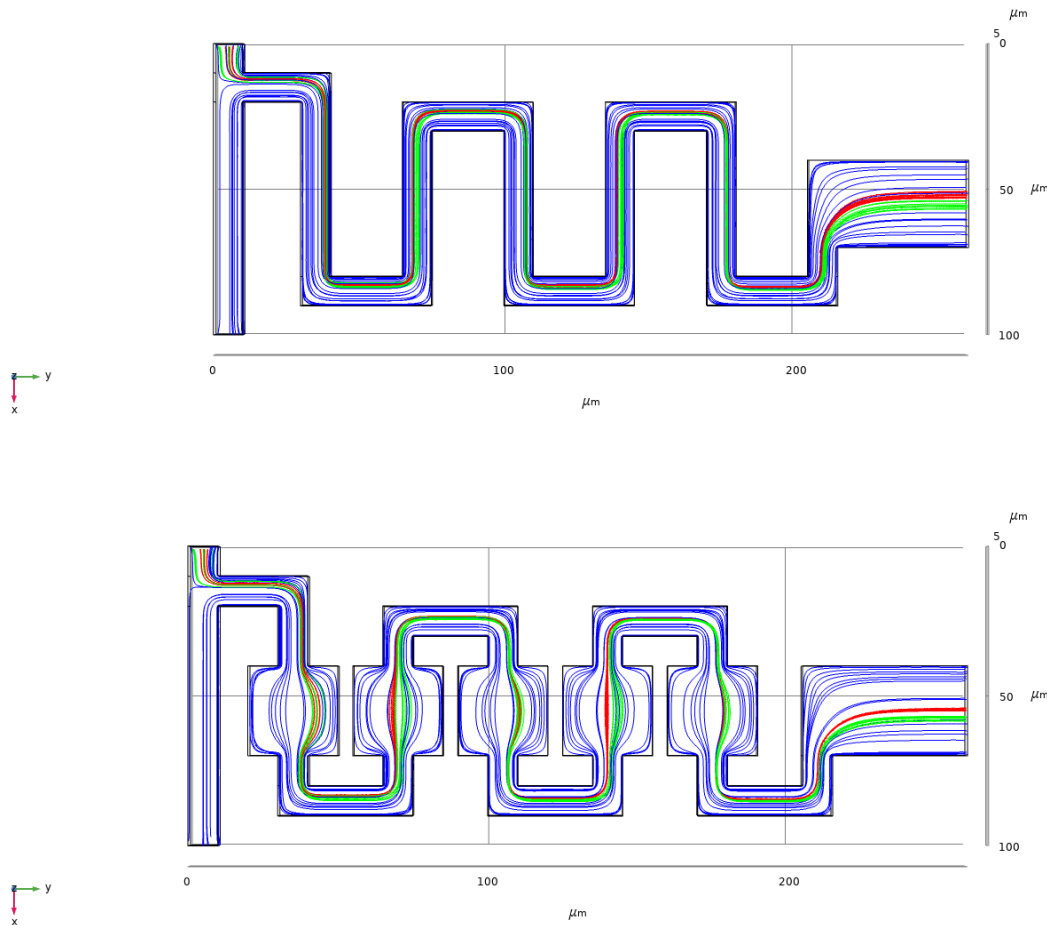


Figure 25. (Top) COMSOL Particle tracing with mass and Streamline results in a serpentine channel without expanding/contracting segments. (Bottom) Particle tracing with mass and Streamline results with expanding/contracting segments.

Secondly the bifurcation system uses an expansion to disperse the streamlines throughout the channel as a result of the velocity gradient. The manipulation of the gradient was refined through the addition of a sink segment to the left of the main channel with respect to the isometric view in Figure 23. Since the sink segment provides another pathway for fluid, it reduces the velocity on the side of the main channel where the sink segment resides. As a result, the shear gradient becomes steeper on that side which in turn causes some stream line to move towards it [JS1]. Figure 26 and Figure 28 showcases the effect of the sink outlet to the velocity gradient and streamlines of the main channel.

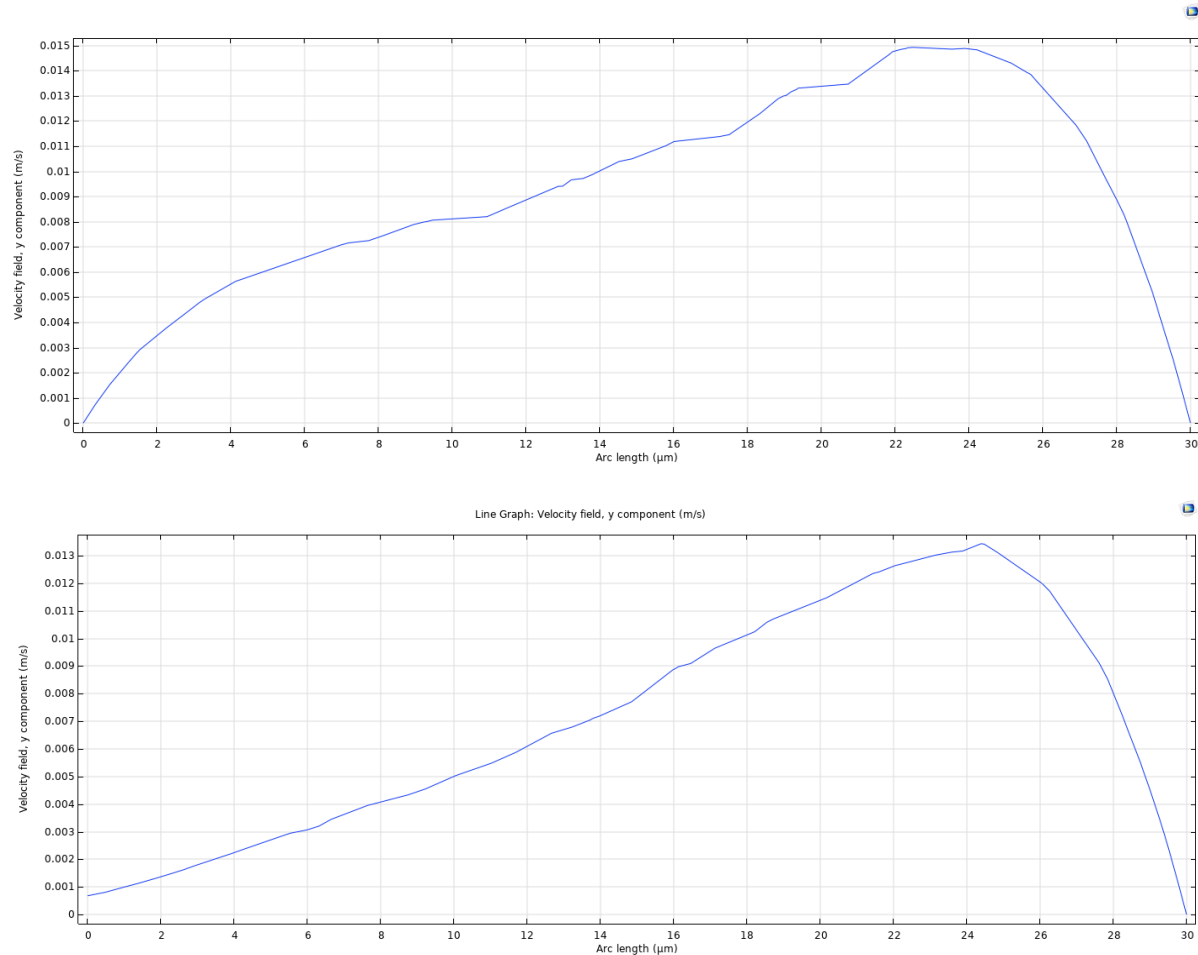


Figure 26. (Top) Velocity gradient of outlet with no sink segment. (bottom) Velocity gradient of outlet with sink segment. (Bottom) Velocity

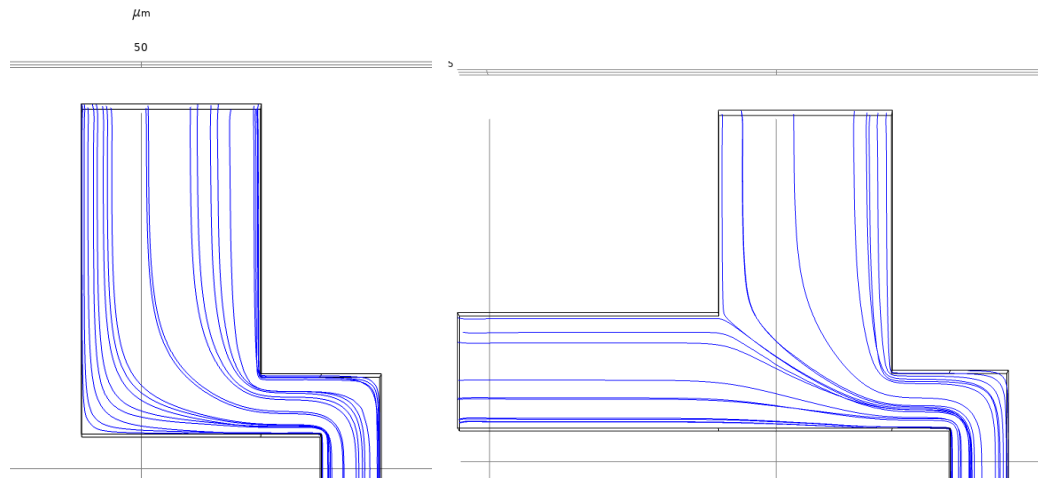
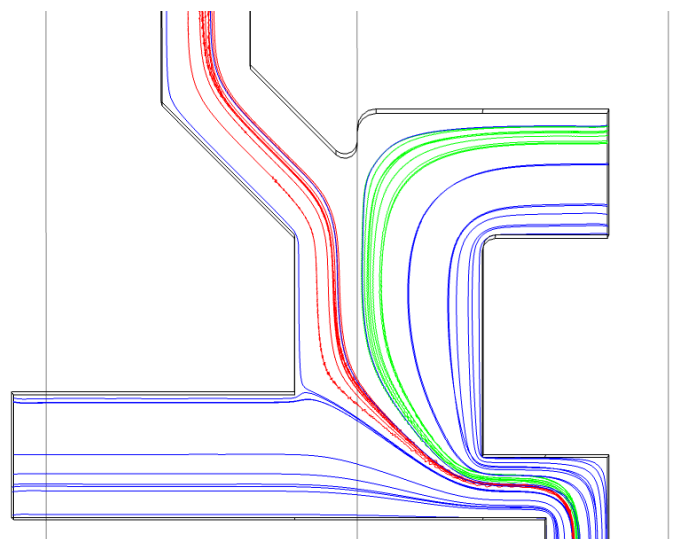


Figure 27. (Top) Velocity gradient of outlet with no sink segment. (bottom) Velocity gradient of outlet with sink segment. (Bottom) Velocity

As a result of the sink segment shown in Figure JS10, the streamlines provided pathways for the particles towards their outlet who's width and length were based on balancing hydraulic resistance to avoid the particles from going to the wrong outlet.



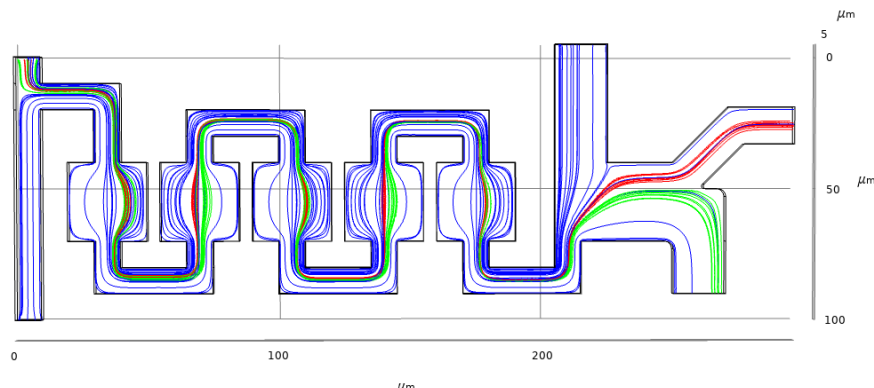


Figure 28. COMSOL particle tracing with mass and streamline results

### 6.3 Concept 3 - Pinched Fractionation with Double Buffer Flow

#### 6.3.1 Initial Design

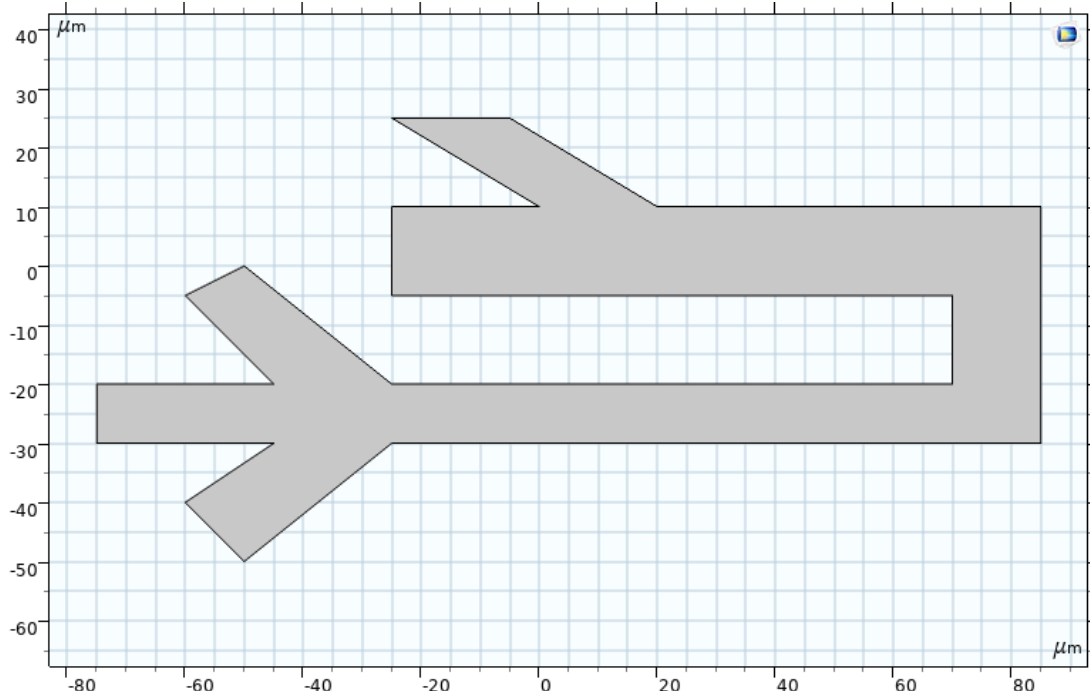


Figure 29. Initial Design of Concept 3

This concept explores the Pinched Flow Fractionation passive technique for particle separation and is 2D simulated using COMSOL simulation software. This design consists of two

inlets and three outlets. The first inlet is for particles insertion and the other inlet acts as a bifurcation channel. The design is 90 $\mu\text{m}$  in width and 75 $\mu\text{m}$  in height with a 20 $\mu\text{m}$  main channel and a 15 $\mu\text{m}$  pinched channel. The outlets are designed to be symmetrical to each other since PFF technique aims to distribute liquid uniformly and have equal fluid resistance in the daughter channels.

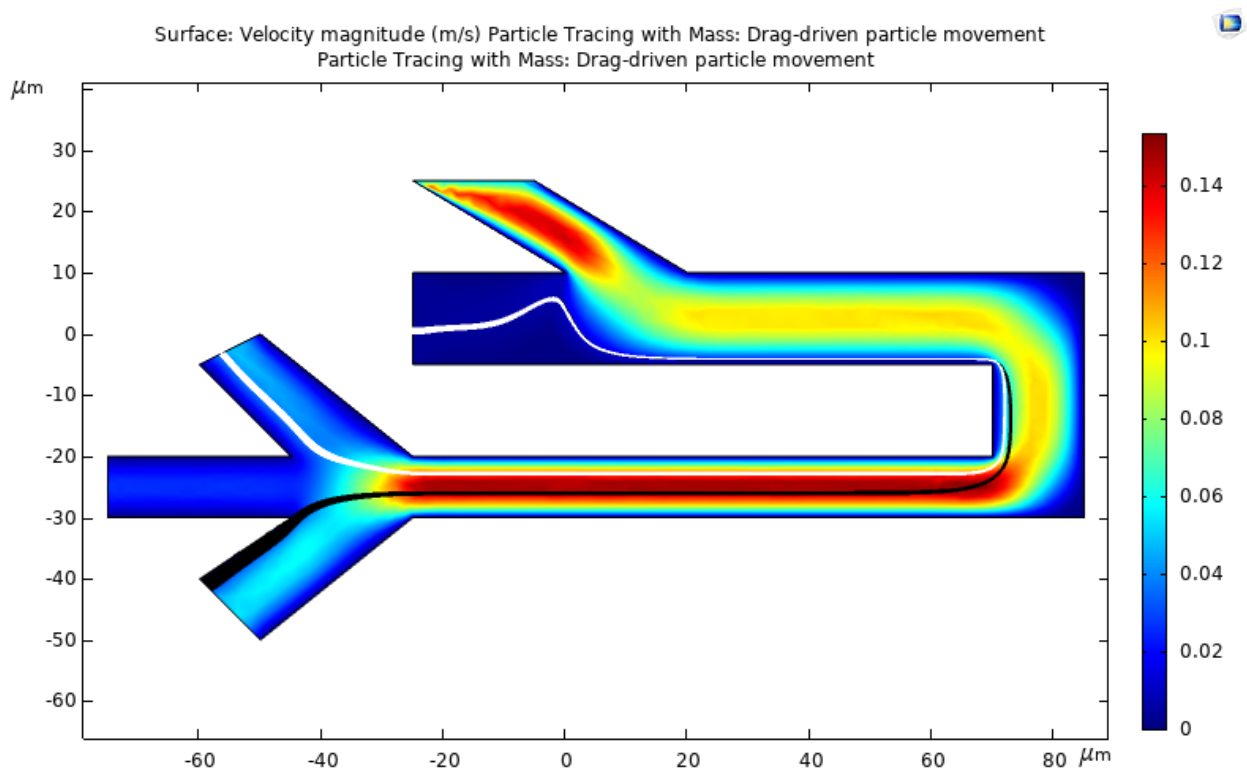


Figure 30. Velocity Plot with Particle Tracing with Mass for Initial Concept 3 - Note: 3.75 $\mu\text{m}$  radius particle - Black, 1.5 $\mu\text{m}$  radius- White

Figure 30 shows the velocity plot of initial concept 3 with particle tracing of 1.5 $\mu\text{m}$  and 3.75 $\mu\text{m}$  radius particles. A buffer flow is added for flow control and to move more dense particles towards the wall to help with the separation technique. The microchannel has two 90 degrees turns which exerts both drag and centrifugal force on particles causing them to separate due to particles having different densities as seen in “Symmetric Serpentine Channel” reference

design. The pinched channel is two times the size of the  $7.5\mu\text{m}$  particle which helps in further increasing the separation distance between particles. A  $7.5\mu\text{m}$  particle has lower density than a  $3\mu\text{m}$  particle, and hence, it flows closer to the wall. Each particle flows to different outlets at the end and the separation distance is estimated to be  $4\mu\text{m}$ .

### 6.3.2 Final Design

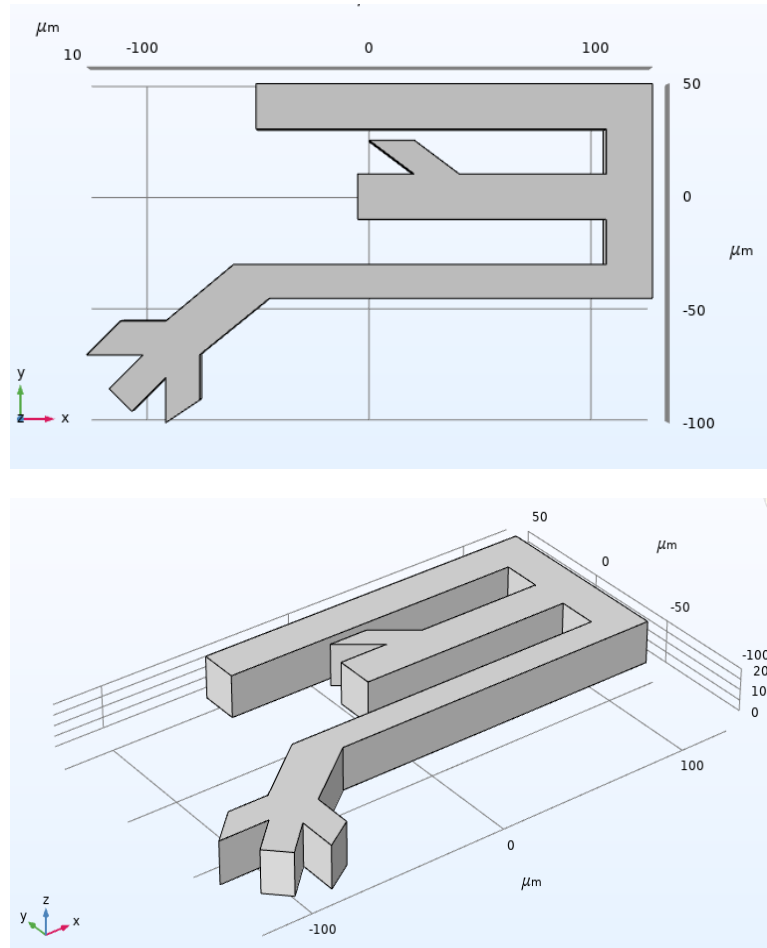


Figure 31. Final Design of Concept 3

In initial concept 3, particles do not separate until they arrive at the pinched channel, which means that the drag and centrifugal forces applied at the corners were not enough to

separate the particles earlier. As a result, the design was altered to be more efficient. In order to further enhance the design and increase particle separation distance, another buffer flow channel was attached to the top of the main channel as shown in Figure 31. In addition, the microchannel was extended and a broader angled section was added after the pinched channel. These changes help control fluid flow and further increase separation distance between particles. The extended angled segment of the channel was added to introduce a sedimentation force on the particles, which would move particles away from the wall and decrease the chances of particle collision with the wall. The sedimentation segment also allows for particles to have a greater separation distance. This final design was modelled in 3D and was  $20\mu\text{m}$  extruded. This allows for the channel to carry more particles and further distribute the flow and forces applied.

## 6.4 Concept 4 - Spiral Microchannel

### 6.4.1 Initial Design

This concept is a slight modification of an existing spiral channel, which itself is a modification of a design used to separate CTC cells ( $20\mu\text{m}$ ) from red and white blood cells ( $6-10\mu\text{m}$ ), so the particles being separated have gotten smaller from the original reference design while still exploiting the same physical phenomena [29]. Note that the design referenced from the paper is halved in the upper channel, due to a flow symmetry in the depth axis, but despite that certain lengths can be modified to test the design's limits. The initial inner radius is 4.5mm, outer radius of 12mm, width of 0.5mm, height of 0.15mm, and inlet/outlet length of 3mm.

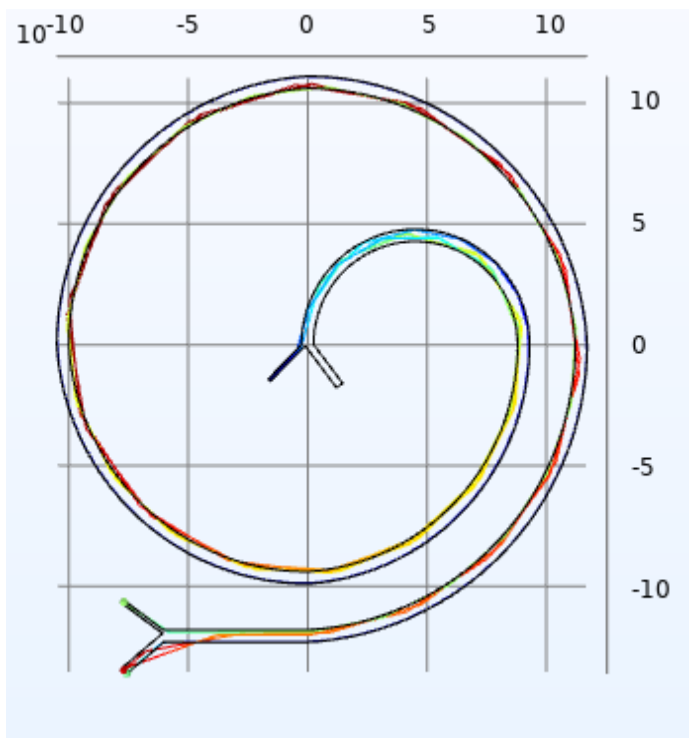
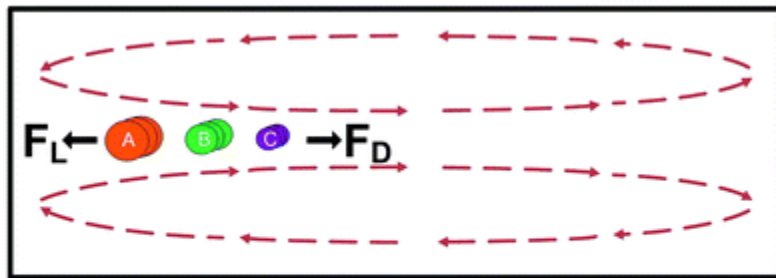


Figure 32: 3D plot of spiral microchannel, Note: 20 $\mu\text{m}$  particle - Light green, 6 $\mu\text{m}$ - Red, 10 $\mu\text{m}$ - Dark green

One of the hard points of this design is the opening width for the 20 $\mu\text{m}$  particle outlet, which is fixed to 0.15mm by design as that's the distance from the channel wall that the particle stays in position. Thanks to the extra 1mm of length at the outlet from the design in the study, the separation distance is roughly 4mm. After some iteration, it was found that the largest particle able to separate was 13 $\mu\text{m}$ . While the design will need to be accommodated for the smaller particle sizes, the Re number is of a bigger concern in the redesign as it's currently at a value of 10. In order to effectively redesign it's first important to expand on Section 2.4.2 in order to get the right formulas that explain the particle's equilibrium position in curvilinear channels like this.

Geometries that exploit the inertial forces in a microchannel in order to achieve a certain equilibrium position of a particle have been replicated with great success [27]. More specifically, curvilinear channels, like in this concept, have been preferred as they form Dean vortices inside the channel that effectively reduce the number of particle equilibrium positions to one, with

separation being achieved by bifurcated outlets [28]. Essentially, particles in a curvilinear channel experience both an inertial lift and Dean drag force, with their magnitude and direction being controlled by the particle size and position within the cross section [28]. Particles following the ratio of  $a_p/D_h \geq 0.07$ , where  $a_p$  is the particle diameter and  $D_h$  is the hydraulic diameter, were of particular importance as they allowed a suitable distance for large particles to be balanced near the channel wall rather than the center for smaller particles, as seen below in Figure 33:



$$\left[ \frac{F_L}{F_D} \right]_A > \left[ \frac{F_L}{F_D} \right]_B > \left[ \frac{F_L}{F_D} \right]_C$$

Figure 33. Inertial lift and drag forces balancing different sized particles [28]

Also noted in Figure 33 are the two counter rotating vortices known as Dean vortices; a product of a centrifugal acceleration component present in the drag force, where it's magnitude is given by Dean number  $De$  (3) and the correlating drag force given by  $F_D$  (4):

$$De = \frac{\rho U_f D_h}{\mu} \sqrt{\frac{D_h}{2R}}$$

$$De = Re \sqrt{\frac{D_h}{2R}} \quad (3) [28]$$

$$F_D = 3\pi\mu U_{Dean} a_p$$

$$F_D = 5.4 \cdot 10^{-4} \pi \mu De^{1.63} a_p \quad (4) [28]$$

Where  $U_f$  is the average flow velocity,  $\mu$  is the fluid viscosity,  $\rho$  is the fluid density,  $R$  is the radius of curvature,  $Re$  is the Reynolds number, and  $U_{\text{Dean}}$  is the average Dean velocity. This coupled with the lift force  $F_L$  (5) for a particle in a plane Poiseuille flow can be used to determine a key correlation between the two opposing forces and particle diameter (Eq. 9):

$$FL = \rho G^2 C_L a_p^4 \quad (5) [28]$$

$$\frac{F_L}{F_D} \propto a_p^3 \quad (9) [28]$$

Where  $G = U_{\max}/D_h$ ,  $U_{\max}$  being the max fluid velocity, and  $C_L$  being the lift coefficient. Using the  $a_p/D_h \geq 0.07$  and (9), specific microchannel cross sections can be developed for particles in range of  $10-20\mu\text{m}$  at a  $Re$  range of 1-100 [28].

#### 6.4.2 Final Design

Using the ratio of  $a_p/D_h \geq 0.07$ , where particle diameter size is  $3\mu\text{m}$  and  $7.5\mu\text{m}$ , it's found that the hydraulic diameter to satisfy both particle sizes is  $4.28E-5\text{m}$ , and if assuming the width remains constant, the height is changed to  $0.0224\text{mm}$  or  $22.4\mu\text{m}$ . Now there are two sets of equations when setting Eq. 3 and Eq. 4, one for each particle size. Assuming the smallest  $Re$  value, the  $U_{\max}$  value can be solved for, given that the lift coefficient  $C_L$  is retrieved from predetermined values of  $Re$  and particle size. But that's where a big issue comes in, as the lowest recorded number of  $Re$  and particle size combinations to find lift forces are  $13.7$  and  $22\mu\text{m}$ , a far cry from the  $1$   $Re$  value needed to be semi-comparable to other concepts, let alone the  $0.1$   $Re$  most run at [30].

While having different sized outlets do allow separation from particles in the  $7.5-10\mu\text{m}$  if the width outlets are dimensioned  $100\mu\text{m}$  and  $200\mu\text{m}$ , it's still not comparable to the assumptions set in Section 5.3. This is simply due to the difference in equilibrium positions not being different enough for said particle sizes at that low of an  $Re$  value. It's better then to keep Concept 1, the inertial focusing with cross flow filters, as relying on pressure difference is more reliable for the particle sizes discussed. Therefore, there's no point in using convergence testing

## 6.5 Concept Evaluation

The concept evaluation is based on the outlined design requirements. The highest priority is given to the functionality requirements. The usability and producibility requirements are secondary to the functionality since the focus is on the geometry and performance of the design. The functionality requirements were that the designs must have a 1000 particle/sec throughput, be able to separate two different sized particles at the micron scale using passive techniques, and have a result deviation lower than 10%. Moreover, the evaluations are based on the outlined system assumptions. The system design assumptions were there is no slip condition at the channel walls, the fluid used is Newtonian and incompressible (specifically, the fluid used is water at 273.15K which indicates the density is density of  $999.8 \text{ kg/m}^3$  and dynamic viscosity of  $1.79 \cdot 10^{-3} \text{ Pa}\cdot\text{s}$ ), and the fluid flow is laminar with a Reynolds number of 0.1. To clarify, for the Reynolds number the characteristic length was defined as the hydraulic diameter which was taken at the coordinate plane of separation and the inlet speed for the flow speed. Also, due to the limitations of COMSOL Multiphysics Simulation Software particle-to-particle collision is ignored and the particles are treated as points as opposed to spheres. The properties of the particles are outlined in Table 1. Regarding rankings, the designs will be evaluated regarding their particle separation distance and meeting the minimum particle throughput.

Table 1. Properties of the Particles

Smaller Particle Diameter ( $\mu\text{m}$ )	3.0
Larger Particle Diameter ( $\mu\text{m}$ )	7.5
Mass of both Particles (kg)	$1 \cdot 10^{-12}$

The methodology used for determining particle separation distance is to average the particle separation distance of the  $3.0\mu\text{m}$  from the  $7.5\mu\text{m}$  diameter particle at a specific coordinate plane in the simulation. To clarify, different starting points were chosen for both particles at the inlet. This was done to cover as many possibilities regarding the path the particles take in the microchannels. Afterwards, the coordinates after the particles crossed the designated separation plane were recorded. The distance between each different sized particle was recorded and calculated using (6):

$$\bar{r} = \sqrt{\Delta x^2 + \Delta y^2 + \Delta z^2} \quad (6)$$

To clarify, the distance for one  $3.0\mu\text{m}$  diameter particle to every other  $7.5\mu\text{m}$  diameter particle was averaged. The tables for the coordinates can be found in Appendix C Tables C1 to C6.

The following relation can be made using the 7.5-to-3.0 ratio the diameters of the particles:

$$1000 = N_{7.5} + N_{3.0} \quad (7a)$$

$$N_{3.0} = \frac{7.5}{3.0}N_{7.5} = 2.5N_{7.5} \quad (7b)$$

$$1000 = 3.5N_{7.5}, N_{7.5} \approx 286 \text{ particles}, N_{3.0} = 714 \text{ particles} \quad (7c)$$

Where N is the number of particles. As per (7b) there are 2.5x more  $3.0\mu\text{m}$  diameter particles relative to the  $7.5\mu\text{m}$  diameter particles. As per (7c) for 1000 particle/sec throughput approximately 714 of them are the  $3.0\mu\text{m}$  diameter particles and 286 of them are the  $7.5\mu\text{m}$  diameter particles. Using the Tables C1 to C6 in Appendix C, the time from start to the separation coordinate plane can be used in the following relation:

$$T = Nt/n \quad (8a)$$

$$T' = T/n_c \quad (8b)$$

For (8a), T is the total time for all the particles in a specific streamline to reach the separation plane, t is the time it takes for one particle to reach the stream line, and n is the number of stream moving in parallel sharing the particle load. For (8a), T' is the total time for all the particles in a specific streamline to reach the separation plane if the particles are clustered together and  $n_c$  is the number of particles clustered together. Thus, sum of T' for all streamlines considered will determine if the throughput is greater than 1000 particles/sec.

The methodology regarding the convergence test is that the simulation was run then it was run again after halving the maximum mesh size. Random coordinate nodes were selected at the regular mesh size along with the velocity at that point. Coordinates close to the initial chosen points at half the maximum mesh size were chosen along with the velocity at that point. The velocities at both maximum mesh sizes were compared to ensure there was less than a 10% difference between the velocities. However, in a real-work setting the difference would have to be less than 1%. This is to ensure the simulation model converges on a solution and is dependent on a physical model as opposed to the number of iterations. If the simulation did not converge the simulation would have to be run again with a denser mesh.

### 6.5.1 Results

Table 2. Concept 1, Average particle separation distance for different starting inlet position of the 3.0 $\mu\text{m}$  diameter particle

Particle Position	Pos. from inlet center in the y-direction [ $\mu\text{m}$ ]	Pos. from inlet center in the z-direction [ $\mu\text{m}$ ]	Abs. Dist. from inlet center [ $\mu\text{m}$ ]	Avg. Separation Dist. per Particle Starting Pos. [ $\mu\text{m}$ ]
1	-12.5	0	12.5	8.47
2	-6.25	0	6.25	6.40
3	0	0	0	5.62
4	6.25	0	6.25	6.32
5	12.5	0	12.5	7.88
7	0	-6.25	6.25	6.34
8	0	0	0	5.57
9	0	6.25	6.25	4.60
10	0	12.5	12.5	3.44
Overall Avg. Separation Dist. [ $\mu\text{m}$ ]				6.07

Table 3. Concept 2, Average particle separation distance for different starting inlet position of the 3.0 $\mu\text{m}$  diameter particle

Particle Position	Pos. from inlet center in the y-direction [ $\mu\text{m}$ ]	Pos. from inlet center in the z-direction [ $\mu\text{m}$ ]	Abs. Dist. from inlet center [ $\mu\text{m}$ ]	Angle [deg]	Avg. Separation Dist. per Particle Starting Pos. [ $\mu\text{m}$ ]
1	3.50	3.50	4.95	45.00	5.94
2	3.50	0.00	3.50	0.00	9.17
3	3.50	-3.50	4.95	315.00	5.76
4	0.00	3.50	3.50	90.00	6.75
5	0.00	0.00	0.00	N/A	9.35
6	0.00	-3.50	3.50	270.00	7.29
7	-3.50	3.50	4.95	135.00	7.33
8	-3.50	0.00	3.50	180.00	9.50
9	-3.50	-3.50	4.95	225.00	7.25
Overall Avg. Separation Dist. [ $\mu\text{m}$ ]					7.59

Table 4. Concept 3, Average particle separation distance for different starting inlet position of the 3.0 $\mu\text{m}$  diameter particle

Particle Position	Pos. from inlet center in the y-direction [ $\mu\text{m}$ ]	Pos. from inlet center in the z-direction [ $\mu\text{m}$ ]	Abs. Dist. from inlet center [ $\mu\text{m}$ ]	Avg. Separation Dist. per Particle Starting Pos. [ $\mu\text{m}$ ]
1.00	-7.50	0.00	7.50	4.05
2.00	-3.75	0.00	3.75	7.03
6.00	0.00	-7.50	7.50	7.46
7.00	0.00	-3.75	3.75	7.52
9.00	0.00	3.75	3.75	8.15
10.00	0.00	7.50	7.50	7.98
Overall Avg. Separation Dist. [ $\mu\text{m}$ ]				7.03

Table 5. Summarized Separation Distance

	Overall Avg. Separation Dist. [ $\mu\text{m}$ ]
Concept 1 - Cross-Flow Filters with Inertial Focusing	6.07
Concept 2 - Serpentine Channel using Buffer Flow	7.59
Concept 3 - Pinched Fractionation with Double Buffer Flow	7.03

Table 6. Summarized Results for Time until 1000 particles pass the separation plane.

	Time [s]
Concept 1 - Cross-Flow Filters with Inertial Focusing	0.97
Concept 2 - Serpentine Channel using Buffer Flow	0.95
Concept 3 - Pinched Fractionation with Double Buffer Flow	0.76

Table 6 indicates that since all the resultant times are under 1 second all concepts achieve the minimum 1000 particles/sec

### 6.5.2 Concept 1

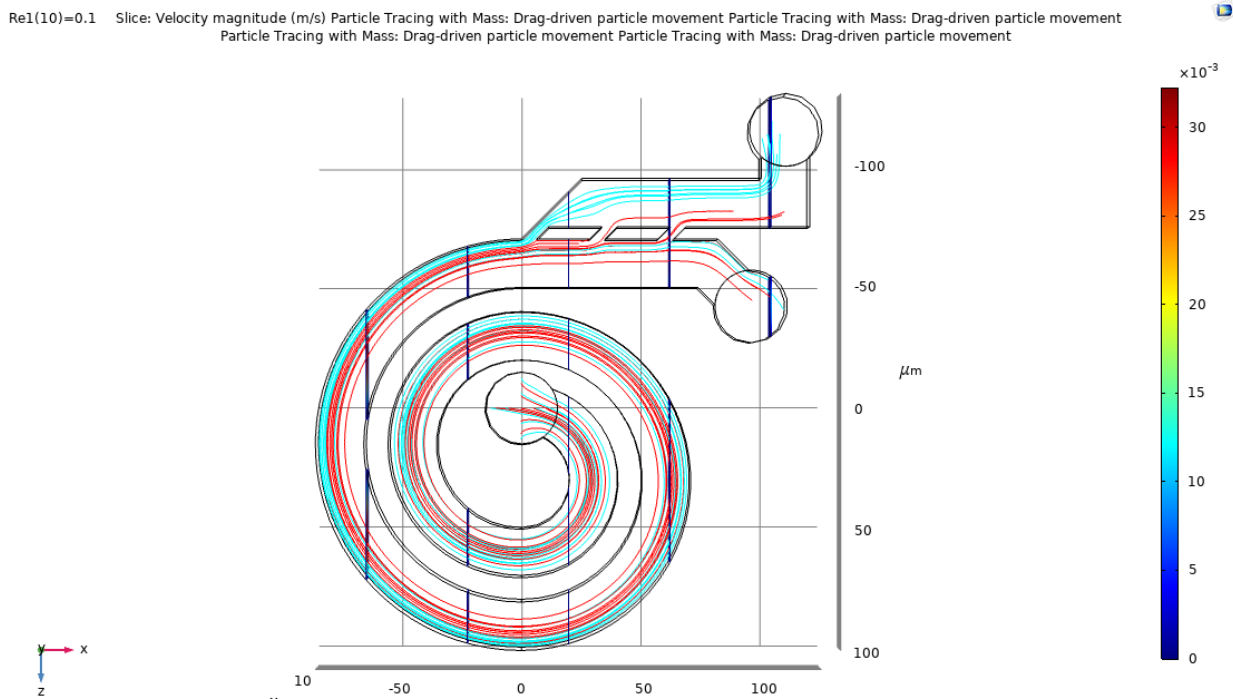


Figure 34. Particle Tracing for Concept 3. Note: 3.75 $\mu\text{m}$  radius particle - Red, 1.5 $\mu\text{m}$  radius particle - Cyan

Figure 34 and 35 show the velocity plot and particle tracing path for Concept 1. As seen in Figure 34, different starting locations for both sized particles were used to gather a range of data for the different paths each of the particles took. However, there is a “blindspot” in the fluid flow that causes particles in its range to collide into the wall. To clarify, a 3.75 $\mu\text{m}$  radius particle was placed at (0, 22, -12.5) and did not make contact with the separation plane. Similarly, a 1.5 $\mu\text{m}$  radius particle placed at (0, 22, -10.25) did not make contact with the separation plane as well. Thus, particles of any size that are released from the inlet closest to the outer spiral wall will not reach the outlets. For the 20 particles released (10 of each) only two not making it correlates to a 10% loss. If the particles are not that dense they may contribute to future clogging or if the particles are very dense they will simply roll off. Also, the simulation has shortcomings due to the assumption that it considers particles as points as opposed to spheres. Being that the cross-flow filters are 6.4 $\mu\text{m}$  wide and the larger (red) particles are 7.5 $\mu\text{m}$  in diameter it is not possible for them to fit through as shown in Figure 34. This indicates that the streamline is

directing some of the larger particles to the second cross-flow filter. This can lead to clogging or membrane fouling at that specific filter. However, this will not interfere too heavily with the filtration since most of the smaller (cyan) particles flow through the first filter.

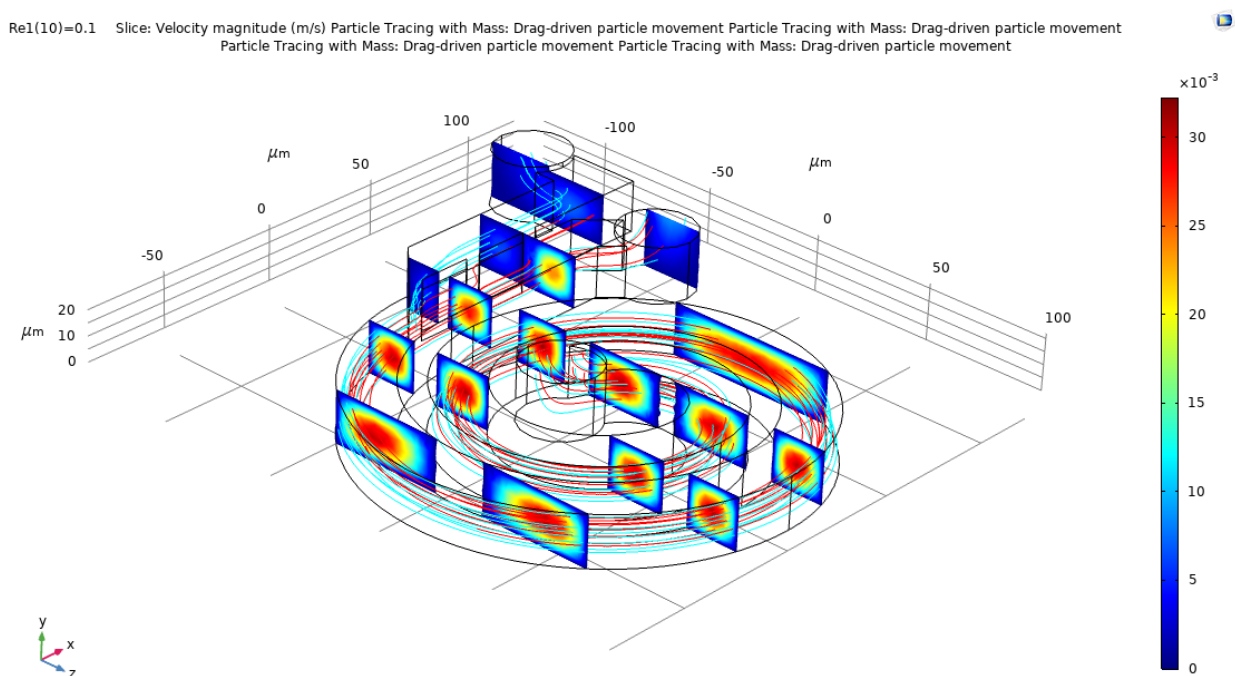


Figure 35. Velocity Plot for Concept 1. Note: 3.75 $\mu\text{m}$  radius particle - Red, 1.5 $\mu\text{m}$  radius- Cyan

Regarding the flow conditions of the geometry, the Reynolds number for the design was 0.1. This implies that the hydraulic diameter at the plane of separation is 20 $\mu\text{m}$  and the inlet velocity is 0.009m/s. For the convergence test the normal maximum mesh size was 4.54 $\mu\text{m}$  and halving it was 2.27 $\mu\text{m}$ . This led to a percentage difference in the velocity profile approximately 3.69%.

Table 7. Percentage Difference of Velocity Results of Convergence Test of Concept 1

Percentage difference (%)			
x-direction	y-direction	z-direction	Velocity profile
0.007%	0.000%	0.314%	5.008%
0.003%	3.754%	0.352%	1.811%
0.015%	0.992%	3.213%	4.240%

### 6.5.3 Concept 2

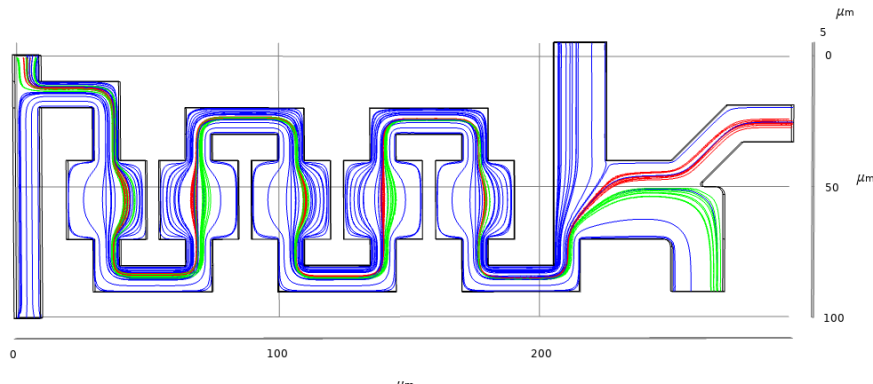


Figure 36. COMSOL particle tracing with mass and streamline results

According to Figure 36 and Figure 37, every particle trajectory managed to reach their respective outlet channels. This was possible due to the avoidance of lengthy wide straight channels and the benefits from the focusing mechanisms employed in the geometry. The lengthy wide straight at low Reynolds number seems to cause smaller and less dense particles to reach 0 velocity midway through the channel. This may be due to the smaller drag forces that smaller particles experience.

Concept 2's overall average separation distance of  $7.59\mu\text{m}$  proves to be the highest in comparison to concept 1 and 3. Based on Table 3, particles starting at the middle of the inlet, depth wise have the highest separation distance with an overall average of  $9.34\mu\text{m}$  out of all the

starting points. This is due to the nature of laminar flow velocity gradient at which the middle section between two walls tends to have the peak velocity compared to other sections of a square cross section. As a consequence to the laminar velocity profile, particles starting at the extreme corners and sides of the inlet prove to have the lower average particle distance in comparison to those at the middle depth of the inlet. Moreover, the standard deviation of the simulated particles' separation distance in Table 3 is  $1.43\mu\text{m}$  which is 18.8% of the overall average particle separation distance. A relatively big standard deviation such as mentioned implies the sensitivity of the initial positions of the particles in relation to their trajectory at the end of the channel.

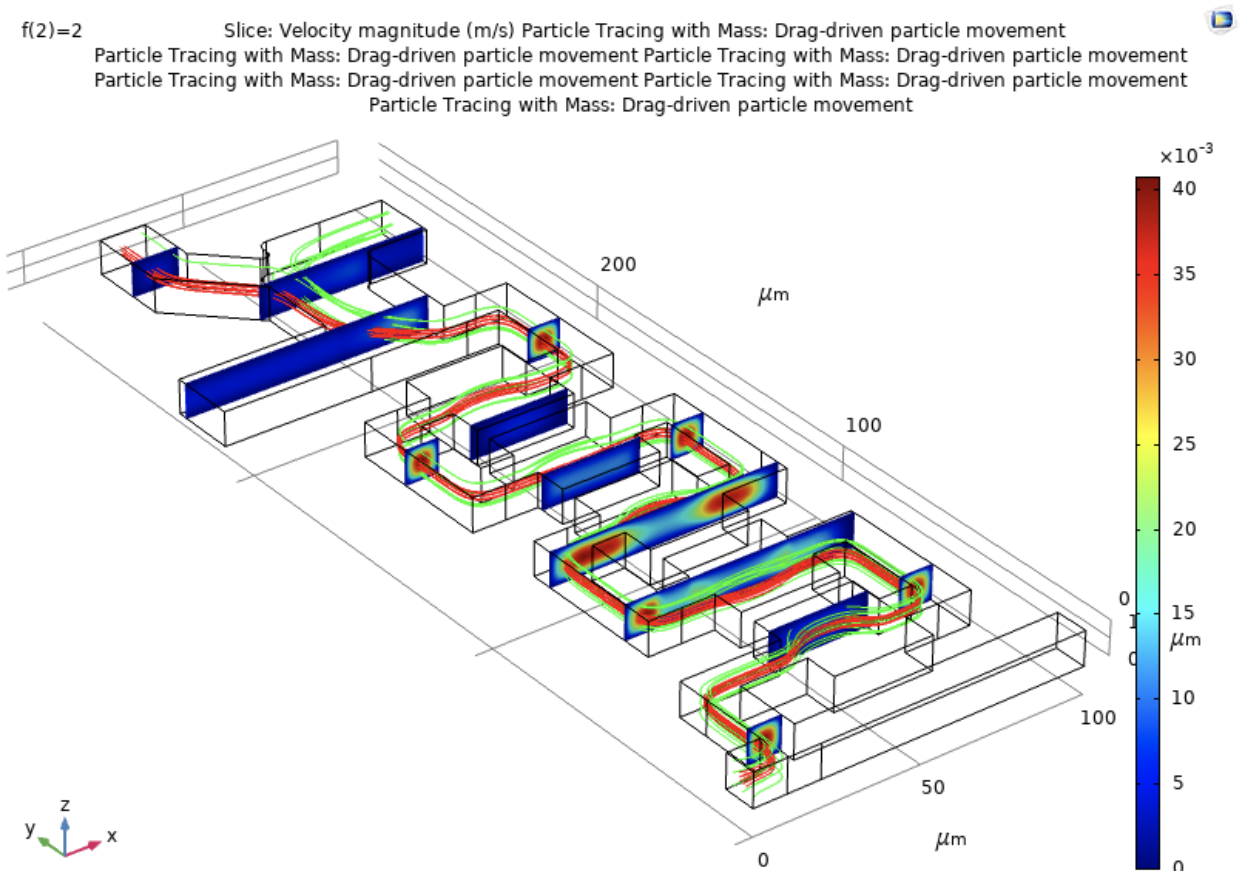


Figure 37. Velocity Plot for Concept 2. Note:  $3.75\mu\text{m}$  radius particle - Red,  $1.5\mu\text{m}$  radius-Green

In terms of flow conditions of the geometry, a Reynolds number 0.1 was decided for the channel at which particles are supposedly fully separate. Therefore the inlet velocities we're

calculated through the continuity equation which resulted in an inlet velocity of 2.0e-2 m/s. Additionally, the geometry was designed around a buffer flow to sample flow inlet velocity ratio of 2:1. In the matter of error in the simulation results, a convergence test was performed at 3 points for fluid velocity which resulted in deviations in Table 8. According to the list of requirements under functionality, the deviation requirement of less than 10% is fulfilled.

Table 8. Percentage Difference of Velocity Results of Convergence Test of Concept 2

Percentage difference (%)			
x-direction	y-direction	z-direction	Velocity profile
0.002	4.063	0.000	1.249
0.001	0.011	0.000	5.575
0.099	0.182	0.000	0.977

#### 6.5.4 Concept 3

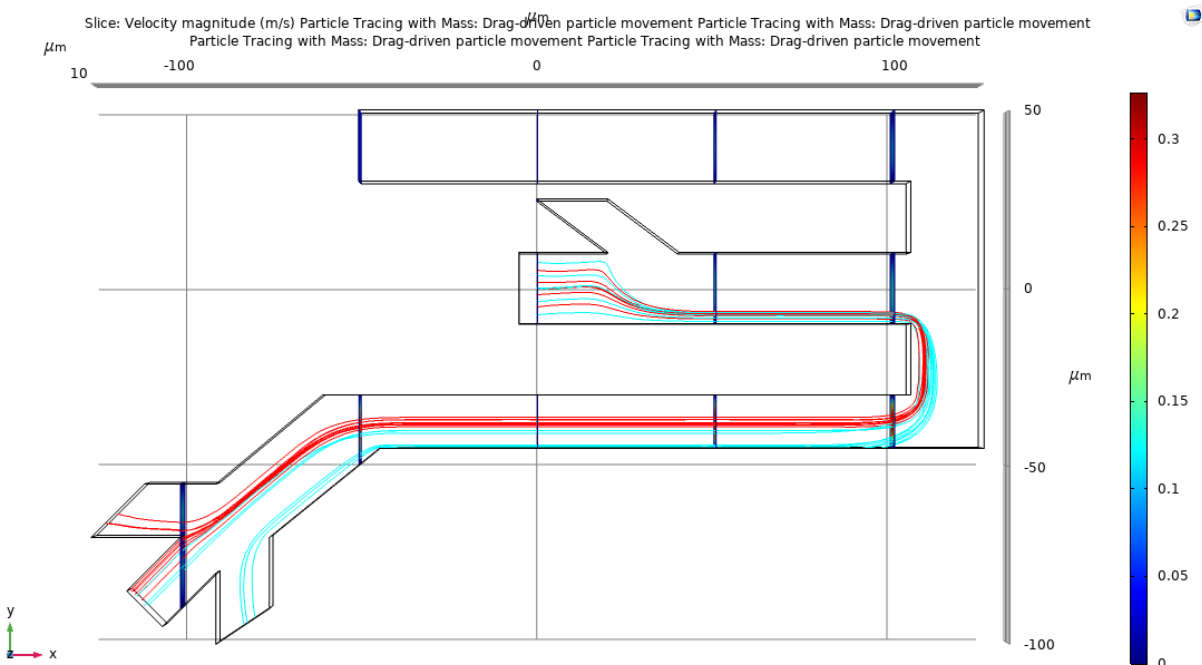


Figure 38. Particle Tracing for Concept 3. Note: 3.75 $\mu\text{m}$  radius particle - Red, 1.5 $\mu\text{m}$  radius particle - Cyan

Figure 38 and Figure 39 show the velocity plot and particle tracing path of Concept 3, which was simulated using COMSOL. As seen in Figure 38, several particles were released from the inlet of the microchannel. Particles were released across the cross-section for a more accurate particle separation distance between streamlines calculation. It was observed that the starting position of the particle affects the particle's path. A few particles were observed to have collided with the wall. For example, the 1.5 $\mu\text{m}$  radius particle 1 released at (0,-7.5,10) near the wall away from the buffer flow channel moved in the same path as the 3.75 $\mu\text{m}$  radius particle streamline. Whereas, the 1.5 $\mu\text{m}$  radius particles 4 and 5 released at (0,7.5,10) and (0,3.75,10) near the buffer channel collided with the wall and did not reach the outlet due to high particle speed. The particle released in the middle of the inlet flowed to its designated outlet with a great separation distance from the 3.75 $\mu\text{m}$  radius particle streamline. Average distance between particles is estimated to be 7.03 $\mu\text{m}$ , which is 43% more than the separation distance of the initial concept.

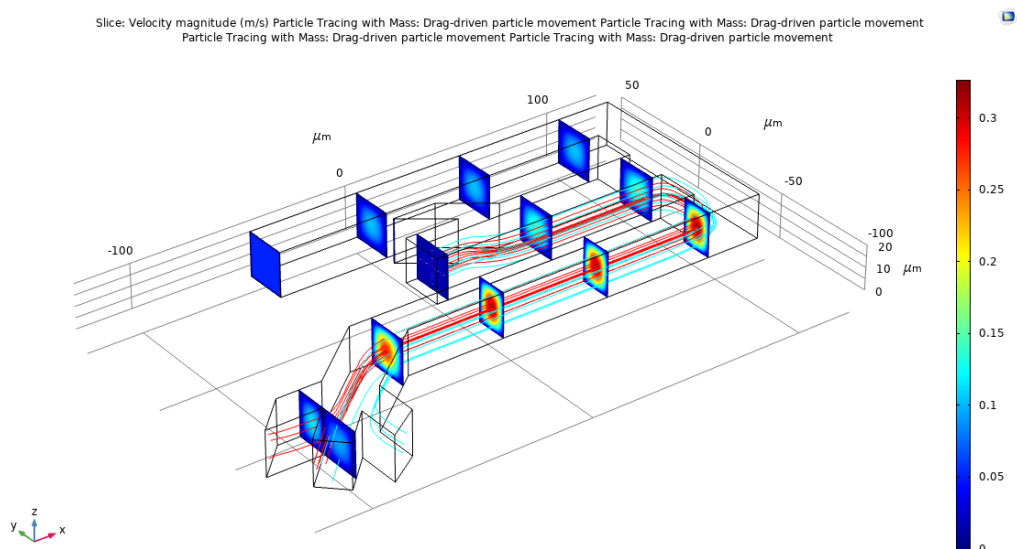


Figure 39. Velocity Plot for Concept 3. Note: 3.75 $\mu\text{m}$  radius particle - Red, 1.5 $\mu\text{m}$  radius- Cyan

Inlet velocity of the channel was calculated using the Reynolds number as shown in Appendix B. Inlet velocity for the particles was calculated to be 0.0105 m/s while for the middle

and top buffer flow channels, the velocities were 0.05 m/s and 0.06 m/s simultaneously. A convergence and mesh test was conducted to ensure that changing the mesh size does not affect the results of the design simulation. For this project, the velocity results were examined in the convergence test. This concept design has a normal mesh element with a maximum size of  $3.67\mu\text{m}$  which was halved to  $1.835\mu\text{m}$  to conduct the test. Velocity speed was examined for both mesh sizes and on average, the percentage difference in velocity for all three dimensions is 1.62%. No velocity change was observed in the x-direction while the biggest percentage difference was seen in the z-axis velocity which would be the cause of forces exerted on the particles in the z-direction. Summary of the convergence test can be seen Table 9.

Table 9. Percentage Difference of Velocity Results of Convergence Test of Concept 3

Percentage difference (%)			
x-direction	y-direction	z-direction	Velocity profile
0	0.013	1.227	1.771
0	0.413	3.696	2.507
0	0.267	1.214	1.155

## 7.0 Conclusion and Recommendations

To sum up, a variety of new passive microfluidic designs were derived from existing passive techniques and compared with similar flow conditions for separation distance, manufacturability, convergence, and throughput. All of these geometries utilize a  $3\mu\text{m}$  and  $7.5\mu\text{m}$  particle sizes for separation (emulating a Thrombocyte and Erythrocytes particles respectively), and are evaluated at  $\text{Re} = 0.1$ . In terms of highest separation distance, Concept 2- Serpentine channel with buffer flow, came in first at  $7.59\mu\text{m}$ , almost 8% larger than second place: Concept 3: PFF with buffer flow. Despite that, Concept 3 did win the highest particle throughput of 0.76 seconds until 1000 particles passed the separation plane, about 20% higher than the second place: Concept 2. All concepts did well in convergence testing, with average percentage differences no higher than 2%. Lastly, in terms of ease of manufacturing, or how much little variation the cross sections in the pattern has, it goes to Concept 2, as it has no angled lines and can be easily made in CAD to be printed as a negative mask.

In terms of recommendations, if the project were to have a wider  $\text{Re}$  range or larger sized particles, a good option would be using the Dean flow fractionation technique on a spiral, due to its large throughput and efficient design. Concept 4 was an example of this and was subsequently scrapped, but could've been a real contender.

## 8.0 References

- [1] B. E. Rapp, *Microfluidics: Modeling, Mechanics and Mathematics.* (1st ed.) 2016.
- [2] P. Sajeesh *et al*, "Particle separation and sorting in microfluidic devices: a review," *Microfluidics and Nanofluidics*, vol. 17, (1), pp. 1-52, 2014.
- [3] C. Church *et al*, "Continuous particle separation in a serpentine microchannel via negative and positive dielectrophoretic focusing," *Journal of Micromechanics and Microengineering*, vol. 20, (6), pp. 065011, 2010.
- [4] N. Pamme and A. Manz, "On-Chip Free-Flow Magnetophoresis: Continuous Flow Separation of Magnetic Particles and Agglomerates," *Analytical Chemistry (Washington)*, vol. 76, (24), pp. 7250-7256, 2004.
- [5] M. Hejazian and N. Nguyen, "Magnetofluidic concentration and separation of non-magnetic particles using two magnet arrays," *Biomicrofluidics*, vol. 10, (4), pp. 044103-044103, 2016.
- [6] P. S. Dittrich and A. Manz, "Lab-on-a-chip: microfluidics in drug discovery," *Nature Reviews. Drug Discovery*, vol. 5, (3), pp. 210-218, 2006.
- [7] M. Schonberger, *Emerging Trends in Medical Plastic Engineering and Manufacturing.* 2016
- [8] R. Daw and J. Finkelstein, "Lab on a chip," *Nature (London)*, vol. 442, (7101), pp. 367-367, 2006.
- [9] S. Chakraborty, *Microfluidics and Microfabrication.* 2010.

- [10] H. N. Joensson and H. Andersson Svahn, "Droplet Microfluidics—A Tool for Single-Cell Analysis," *Angewandte Chemie (International Ed.)*, vol. 51, (49), pp. 12176-12192, 2012.
- [11] W. K. T. Coltro et al, "Toner and paper-based fabrication techniques for microfluidic applications," *Electrophoresis*, vol. 31, (15), pp. 2487-2498, 2010.
- [12] I. U. Khan et al, "Production of nanoparticle drug delivery systems with microfluidics tools," *Expert Opinion on Drug Delivery*, vol. 12, (4), pp. 547-562, 2015.
- [13] N. Nguyen, S. T. Wereley and S. A. M. Shaegh, *Fundamentals and Applications of Microfluidics*. (Third ed.) 2019.
- [14] "Multiphysics Cyclopedia," COMSOL. [Online]. Available: <https://www.comsol.com/multiphysics/navier-stokes-equations?parent=modeling-conservation-mass-energy-momentum-0402-432-302>. [Accessed: 11-Feb-2021].
- [15] J. Picot et al, "Flow cytometry: retrospective, fundamentals and recent instrumentation," *Cytotechnology (Dordrecht)*, vol. 64, (2), pp. 109-130, 2012.
- [16] M. J. Jaroszeski and G. Radcliff, "Fundamentals of flow cytometry," *Molecular Biotechnology*, vol. 11, (1), pp. 37-53, 1999.
- [17] J. P. Golden et al, "Hydrodynamic focusing—a versatile tool," *Analytical and Bioanalytical Chemistry*, vol. 402, (1), pp. 325-335, 2012.
- [18] E. Pariset et al, "Anticipating Cutoff Diameters in Deterministic Lateral Displacement (DLD) Microfluidic Devices for an Optimized Particle Separation", vol 13, (37), 2017.

- [19] M. Bayareh, "An updated review on particle separation in passive microfluidic devices", *Chemical Engineering and Processing - Process Intensification*, vol 153, 2020.
- [20] "Multiphysics Cyclopedia," *COMSOL*. [Online]. Available: <https://www.comsol.com/multiphysics/fea-software?parent=finite-element-method-042-62-22>. [Accessed: 13-Feb-2021].
- [21] K. Brower, A. K. White and P. M. Fordyce, "Multi-step Variable Height Photolithography for Valved Multilayer Microfluidic Devices," *Journal of Visualized Experiments : JoVE*, (119), 2017.
- [22] Anonymous "3D printed self-supporting elastomeric structures for multifunctional microfluidics," *Science Advances*, vol. 6, (41), 2020.
- [23] Y. Chiu, C. Huang and Y. Lu, "Enhancement of microfluidic particle separation using cross-flow filters with hydrodynamic focusing," *Biomicrofluidics*, vol. 10, (1), pp. 011906-011906, 2016.
- [24] N. Xiang, Q. Li and Z. Ni, "Combining Inertial Microfluidics with Cross-Flow Filtration for High-Fold and High-Throughput Passive Volume Reduction," *Analytical Chemistry (Washington)*, vol. 92, (9), pp. 6770-6776, 2020.
- [25] Z. Jun, "Particle inertial focusing and separation in serpentine microchannels: mechanisms and applications," Doctor of Philosophy thesis, School of Mechanical, Materials and Mechatronic Engineering, University of Wollongong, 2015. <https://ro.uow.edu.au/theses/4492>
- [26] T. Morijiri *et al.* "Sedimentation pinched-flow fractionation for size- and density-based particle sorting in microchannels" Springer Verlag. doi:10.1007/s10404-011-0785-6
- [27] A. A. S. BHAGAT, S. S. KUNTAEGOWDANAHAlli and I. PAPAUTSKY, "Inertial microfluidics for continuous particle filtration and extraction," *Microfluidics and Nanofluidics*, vol. 7, (2), pp. 217-226, 2009.

- [28] S. S. Kuntaegowdanahalli *et al*, "Inertial microfluidics for continuous particle separation in spiral microchannels," *Lab on a Chip*, vol. 9, (20), pp. 2973-2980, 2009.
- [29] H. W. Hou *et al*, "Isolation and retrieval of circulating tumor cells using centrifugal forces," *Scientific Reports*, vol. 3, (1), pp. 1259-1259, 2013.
- [30] S. S. Deshpande, "Measurement of Slip Velocity and Lift Coefficient for Laterally Focused Particles in an Inertial Flow through a Spiral Microfluidic Channel." , ProQuest Dissertations Publishing, 2016.
- [31] F. M. White, *Fluid Mechanics*. (Eighth ed.) McGraw-Hill Education, 2016.
- [32] Y. Chiu, C. Huang and Y. Lu, "Enhancement of microfluidic particle separation using cross-flow filters with hydrodynamic focusing," *Biomicrofluidics*, vol. 10, (1), pp. 011906-011906, 2016.
- [32] N. Xiang, Q. Li and Z. Ni, "Combining Inertial Microfluidics with Cross-Flow Filtration for High-Fold and High-Throughput Passive Volume Reduction," *Analytical Chemistry (Washington)*, vol. 92, (9), pp. 6770-6776, 2020.
- [33] C. Liu *et al*, "A generalized formula for inertial lift on a sphere in microchannels," *Lab on a Chip*, vol. 16, (5), pp. 884-892, 2016.
- [34] L. I. Amar *et al*, "Co-current crossflow microfiltration in a microchannel," *Biomedical Microdevices*, vol. 21, (1), pp. 1-6, 2019.

## 9.0 Appendix A: Detailed Design Drawings

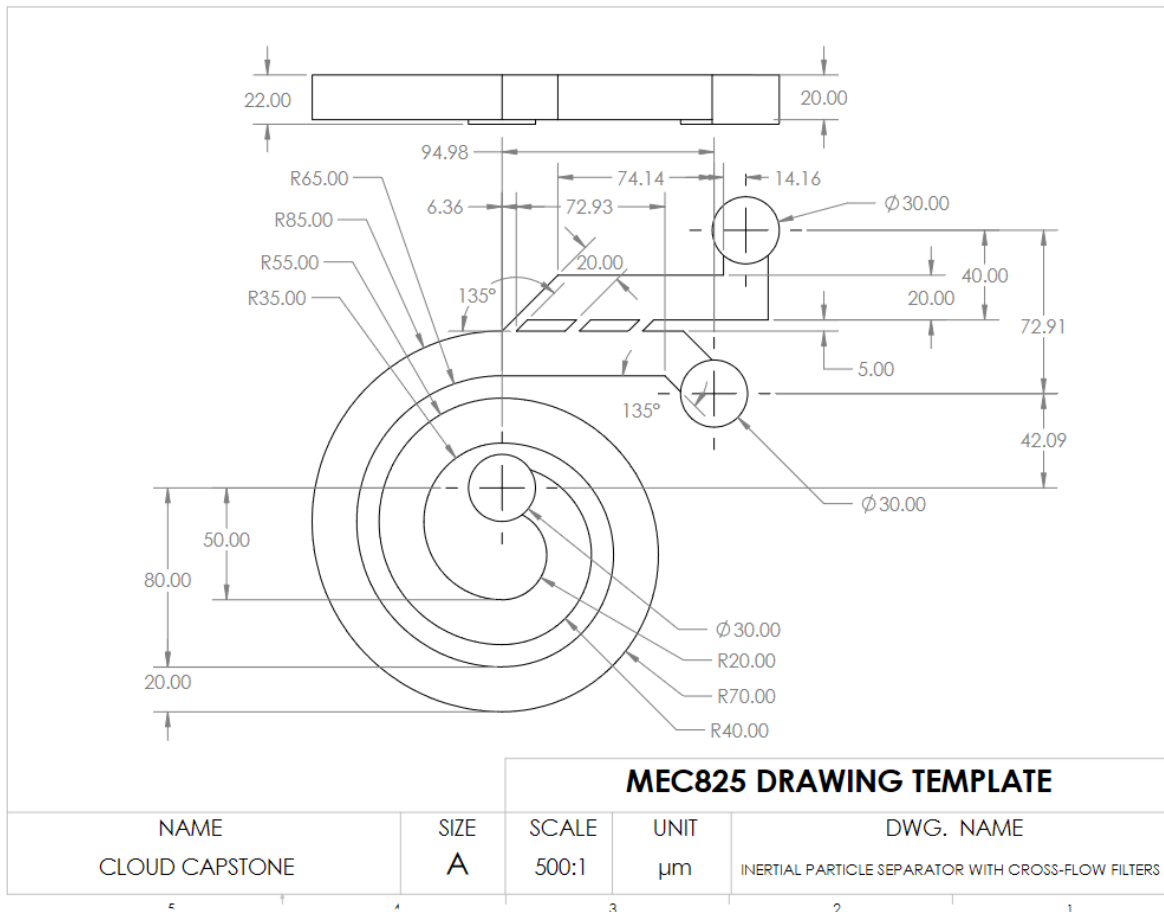


Figure 40. Detailed Drawing of Concept 1

## Concept 2

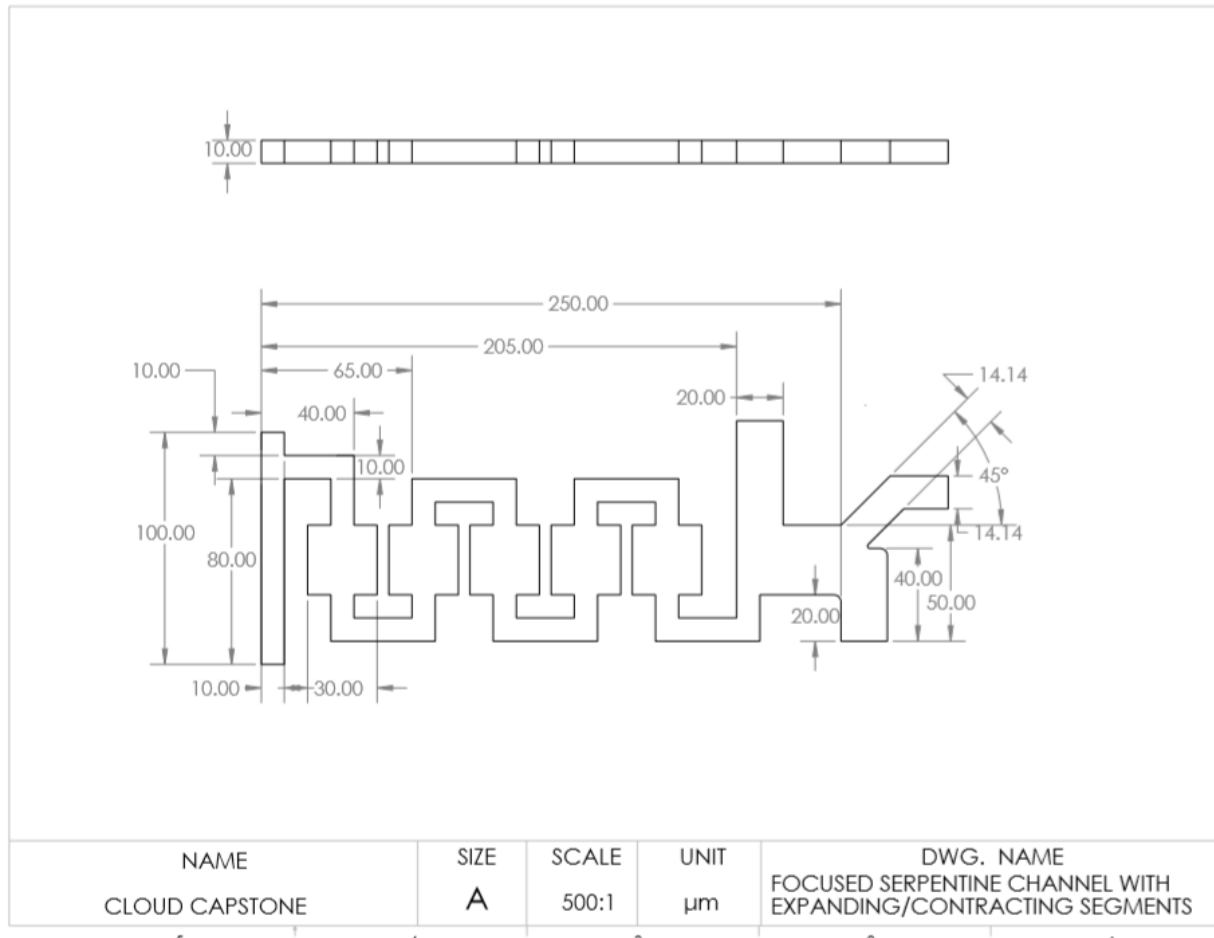


Figure 41. Detailed Drawing of Concept 2

### Concept 3

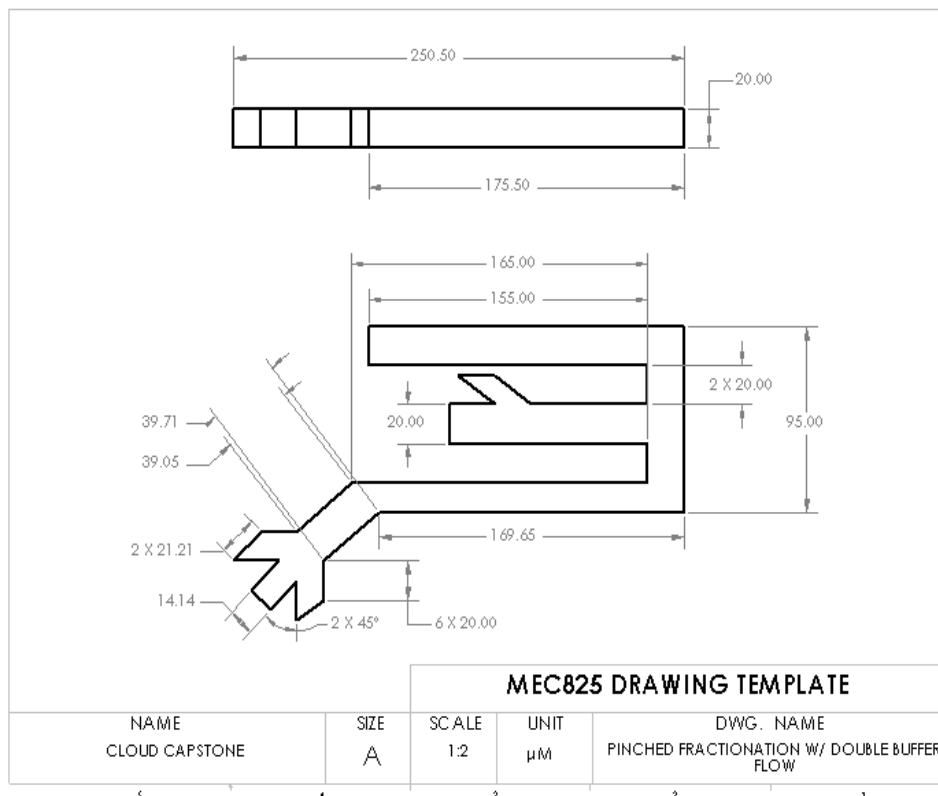


Figure 42. Detailed Drawing of Concept 3

## 10.0 Appendix B: Sample Calculations of Simulation

### Concept 1

Hydraulic Diameter:

$$D_h = \frac{2ab}{a+b} = \frac{2(20 \cdot 10^{-6})(20 \cdot 10^{-6})}{(20 \cdot 10^{-6}) + (20 \cdot 10^{-6})} = 20 \cdot 10^{-6} m$$

Inlet Velocity:

$$V = \frac{Re\mu}{\rho D_h} = \frac{(0.1)(1.8 \cdot 10^{-3})}{(999.8)(20 \cdot 10^{-6})} = 9.00 \cdot 10^{-3} m/s$$

### Concept 2

Hydraulic Diameter:

$$D_h = \frac{2ab}{a+b} = \frac{2(30 \cdot 10^{-6})(10 \cdot 10^{-6})}{(30 \cdot 10^{-6}) + (10 \cdot 10^{-6})} = 15 \cdot 10^{-6} m$$

Inlet Velocity:

$$V_1 = V_2 A_2 / A_1 = \frac{Re\mu A_2}{\rho D_h A_1} = \frac{\mu A_2}{\rho D_h A_1} = 2 \cdot 10^{-2} m$$

### Concept 3

Hydraulic Diameter:

$$D_h = \frac{2ab}{a+b} = \frac{2(15 \cdot 10^{-6})(20 \cdot 10^{-6})}{(15 \cdot 10^{-6}) + (20 \cdot 10^{-6})} = 17 \cdot 10^{-6} m$$

Inlet Velocity:

$$V = \frac{Re\mu}{\rho D_h} = \frac{(0.1)(1.8 \cdot 10^{-3})}{(999.8)(17 \cdot 10^{-6})} = 0.0105 m/s$$

### Concept 4 (Initial Design)

Hydraulic Diameter:

$$D_h = \frac{2ab}{a+b} = \frac{2(5 \cdot 10^{-4})(1.5 \cdot 10^{-5})}{(15 \cdot 10^{-6}) + (1.5 \cdot 10^{-5})} = 4.285 \cdot 10^{-5} m$$

Inlet Velocity:

$$Re = \frac{\rho V D}{\mu} = \frac{(999.8)(0.42m/s)(4.285 \cdot 10^{-5} m)}{(1.8 \cdot 10^{-3})} = 9.99$$

## 11.0 Appendix C: Data Tables

Table C1. Concept 1, 3.0 $\mu\text{m}$ -diameter Particle Coordinates at Inlet and Penetration of Separation Coordinate Plane

3.0E-06 Position	X <sub>1</sub>	Y <sub>1</sub>	Z <sub>1</sub>	Time <sub>1</sub>	X <sub>2</sub>	Y <sub>2</sub>	Z <sub>2</sub>	Time <sub>2</sub>
1	-12.500	22.000	0.000	0.000	0.269	2.259	-63.205	0.053
2	-6.250	22.000	0.000	0.000	0.044	6.292	-68.053	0.039
3	0.000	22.000	0.000	0.000	0.128	10.401	-68.966	0.045
4	6.250	22.000	0.000	0.000	0.123	13.728	-68.887	0.048
5	12.500	22.000	0.000	0.000	0.098	17.214	-67.700	0.068
6	0.000	22.000	-12.500	0.000				
7	0.000	22.000	-6.250	0.000	0.025	8.778	-69.523	0.069
8	0.000	22.000	0.000	0.000	0.069	10.380	-68.899	0.044
9	0.000	22.000	6.250	0.000	0.303	10.723	-67.685	0.031
10	0.000	22.000	12.500	0.000	0.430	9.489	-64.589	0.024

Table C2. Concept 1, 7.5 $\mu\text{m}$ -diameter Particle Coordinates at Inlet and Penetration of Separation Coordinate Plane

7.5E-06 Position	X <sub>1</sub>	Y <sub>1</sub>	Z <sub>1</sub>	Time <sub>1</sub> [s]	X <sub>2</sub>	Y <sub>2</sub>	Z <sub>2</sub>	Time <sub>2</sub> [s]
1	-10.250	22.000	0.000	0.000	0.172	4.238	-62.655	0.034
2	-5.125	22.000	0.000	0.000	0.194	7.526	-64.510	0.027
3	0.000	22.000	0.000	0.000	0.209	10.690	-64.951	0.025
4	5.125	22.000	0.000	0.000	0.271	13.297	-65.589	0.029
5	10.250	22.000	0.000	0.000	0.085	15.892	-66.138	0.041
6	0.000	22.000	-10.250	0.000				
7	0.000	22.000	-5.125	0.000	0.123	9.523	-67.057	0.033
8	0.000	22.000	0.000	0.000	0.028	10.715	-65.016	0.026
9	0.000	22.000	5.125	0.000	0.162	11.072	-62.719	0.023
10	0.000	22.000	10.250	0.000	0.053	10.628	-59.493	0.022

Table C3. Concept 2, 3.0 $\mu\text{m}$ -diameter Particle Coordinates at Inlet and Penetration of Separation Coordinate Plane

3.0E-06 Position	X <sub>1</sub>	Y <sub>1</sub>	Z <sub>1</sub>	Time <sub>1</sub> [s]	X <sub>2</sub>	Y <sub>2</sub>	Z <sub>2</sub>	Time <sub>2</sub> [s]
1	1.000	8.500	8.500	0.000	50.168	250.041	8.217	0.046
2	1.000	8.500	5.000	0.000	54.420	250.026	4.999	0.029
3	1.000	8.500	1.500	0.000	49.961	250.020	1.786	0.046
4	1.000	5.000	8.500	0.000	51.244	250.060	8.002	0.039
5	1.000	5.000	5.000	0.000	54.605	250.042	4.985	0.026
6	1.000	5.000	1.500	0.000	51.800	250.072	1.857	0.040
7	1.000	1.500	8.500	0.000	51.924	250.008	7.948	0.038
8	1.000	1.500	5.000	0.000	54.747	250.104	5.030	0.027
9	1.000	1.500	1.500	0.000	51.855	250.085	2.058	0.037

Table C4. Concept 2, 7.5 $\mu\text{m}$ -diameter Particle Coordinates at Inlet and Penetration of Separation

## Coordinate Plane

7.5E-06 Position	X <sub>1</sub>	Y <sub>1</sub>	Z <sub>1</sub>	Time <sub>1</sub> [s]	X <sub>2</sub>	Y <sub>2</sub>	Z <sub>2</sub>	Time <sub>2</sub> [s]
1	1.000	6.250	6.250	0.000	45.222	250.025	6.026	0.030
2	1.000	6.250	5.000	0.000	45.581	250.040	4.977	0.028
3	1.000	6.250	3.750	0.000	42.895	250.102	3.899	0.032
4	1.000	5.000	6.250	0.000	46.085	250.029	6.056	0.028
5	1.000	5.000	5.000	0.000	46.440	250.011	4.980	0.027
6	1.000	5.000	3.750	0.000	44.462	250.009	3.943	0.029
7	1.000	3.750	6.250	0.000	43.177	250.034	6.047	0.030
8	1.000	3.750	5.000	0.000	46.781	250.020	4.982	0.026
9	1.000	3.750	3.750	0.000	46.955	250.036	3.986	0.027

Table C5. Concept 3, 3.0 $\mu\text{m}$ -diameter Particle Coordinates at Inlet and Penetration of Separation Coordinate Plane

3.0E-06 Position	X <sub>1</sub>	Y <sub>1</sub>	Z <sub>1</sub>	Time <sub>1</sub> [s]	X <sub>2</sub>	Y <sub>2</sub>	Z <sub>2</sub>	Time <sub>2</sub> [s]
1	0.000	-7.500	10.000	0.000	-41.533	-41.268	10.033	0.006
2	0.000	-3.750	10.000	0.000	-40.224	-44.516	10.042	0.006
3	0.000	0.000	10.000	0.000				
4	0.000	3.750	10.000	0.000				
5	0.000	7.500	10.000	0.000				
6	0.000	0.000	2.500	0.000	-41.301	-40.273	2.840	0.005
7	0.000	0.000	6.250	0.000	-40.570	-44.344	6.569	0.005
8	0.000	0.000	10.000	0.000				
9	0.000	0.000	13.750	0.000	-40.206	-44.761	13.501	0.009
10	0.000	0.000	17.500	0.000	-41.664	-40.345	17.137	0.005

Table C6. Concept 3, 7.5 $\mu\text{m}$ -diameter Particle Coordinates at Inlet and Penetration of Separation Coordinate Plane

7.5E-06 Position	X <sub>1</sub>	Y <sub>1</sub>	Z <sub>1</sub>	Time <sub>1</sub> [s]	X <sub>2</sub>	Y <sub>2</sub>	Z <sub>2</sub>	Time <sub>2</sub> [s]
1	0.000	-5.250	10.000	0.000	-41.403	-36.459	10.025	0.004
2	0.000	-2.625	10.000	0.000	-40.488	-37.459	10.047	0.003
3	0.000	0.000	10.000	0.000	-40.018	-38.355	9.983	0.003
4	0.000	2.625	10.000	0.000	-40.929	-38.777	10.008	0.003
5	0.000	5.250	10.000	0.000	-41.253	-39.152	9.989	0.003
6	0.000	0.000	4.750	0.000	-41.646	-37.015	5.330	0.004
7	0.000	0.000	7.375	0.000	-40.416	-38.061	7.727	0.003
8	0.000	0.000	10.000	0.000	-40.570	-38.412	9.994	0.003
9	0.000	0.000	12.625	0.000	-41.970	-37.881	12.248	0.003
10	0.000	0.000	15.250	0.000	-40.621	-37.119	14.602	0.004

## 12.0 Appendix D: Particle Throughput Calculations

Using (8a), (8b), Table C1 to C6 for the time value (t) for 3.0 $\mu\text{m}$  diameter particles

- For Concept 1,  $n = 9$  since as per Table C1 to C6 only 90% of the particles made the separation plane for the 3.0 $\mu\text{m}$  diameter particles
- The N value of 714 is divided by 9 since there are 9 streams that share the particle load considered as per Table C1 to C6 for the 3.0 $\mu\text{m}$  diameter particles for Concept 1

$$T = Ntn = 714/9 \cdot 0.024s = 1.904s$$

- Assuming 2 3.0 $\mu\text{m}$  diameter particles compact and travel together along the path:

$$T' = T/n_c = 1.904/2 = 0.952s$$

- Thus, the time for 1000 particles to pass in Concept 1 is 0.952s

## 13.0 Appendix E: Convergence Test Calculations

Velocity values were taken from slice velocity plot on COMSOL. Percentage difference was calculated to verify if designs are convergent.

Sample calculation for concept 1:

$$\frac{|V_{x1} + V_{x2}|}{((V_{x1} + V_{x2})/2)} = \frac{|-22.25 + (-22.57)|}{(-22.25 - 22.57)/2} \times 100 = 0.003\%$$